DAHLGREN DIVISION
NAVAL SURFACE WARFARE CENTER
Dahlgren, Virginia 22448-5100

NSWCDD/TR-95/107

IMPLEMENTATION AND APPLICATION OF THE P-α EQUATION OF STATE IN THE DYSMAS CODE

ANDREW B. WARDLAW, JR.
SYSTEMS RESEARCH AND TECHNOLOGY DEPARTMENT

REID McKEOWN AND HOWARD CHEN
WARHEAD DYNAMICS DIVISION, NSWC INDIAN HEAD

MAY 1996

REPORT DOCUMENTATION PAGE

Form Approved
OBM No. 0704-0188

1. AGENCY USE ONLY (*Leave blank*)	2. REPORT DATE	3. REPORT TYPE AND DATES COVERED
	May 1996	

4. TITLE AND SUBTITLE
Implementation and Application of the P-α Equation of State in the DYSMAS Code

5. FUNDING NUMBERS

6. AUTHOR(s)
Andrew B. Wardlaw, Jr.

7. PERFORMING ORGANIZATION NAME(S) AND ADDRESS(ES)
Commander
Naval Surface Warfare Center, Dahlgren Division (Code B44)
17320 Dahlgren Road
Dahlgren, VA 22448-5100

8. PERFORMING ORGANIZATION REPORT NUMBER
NSWCDD/TR-95/107

9. SPONSORING/MONITORING AGENCY NAME(S) AND ADDRESS(ES)

10. SPONSORING/MONITORING AGENCY REPORT NUMBER

11. SUPPLEMENTARY NOTES

12a. DISTRIBUTION/AVAILABILITY STATEMENT
Authorized for public release; distribution is unlimited.

12b. DISTRIBUTION CODE

13. ABSTRACT (Maximum 200 words)

This report describes the implementation of the Mie-Gruneisen and P-α equations of state in the DYSMAS code. The motivation for these enhancements is to provide an equation of state that treats partially saturated sand. The pores in the P-α model are used to simulate the sand pore volume free from water, while the Mie-Gruneisen equation of state accounts for the water-grain mixture. Additionally, the Mie-Gruneisen equations of state provides a means of modeling the equations of state of metals.

14. SUBJECT TERMS
DYSMAS Code

15. NUMBER OF PAGES
73

16. PRICE CODE

17. SECURITY CLASSIFICATION OF REPORT	18. SECURITY CLASSIFICATION OF THIS PAGE	19. SECURITY CLASSIFICATION OF ABSTRACT	20. LIMITATION OF ABSTRACT
UNCLASSIFIED	UNCLASSIFIED	UNCLASSIFIED	SAR

FOREWORD

This report describes the implementation of the Mie-Grueneisen and P-α equations of state in the DYSMAS code. The motivation for these enhancements is to provide an equation of state that treats partially saturated sand. The pores in the P-α model are used to simulate the sand pore volume free from water, while the Mie-Grueneisen equation of state accounts for the water-grain mixture. Additionally, the Mie-Grueneisen equations of state provides a means of modeling the equations of state of metals.

This report was sponsored by the Office of Naval Research, Code 3300, under the Undersea Warheads and Explosive and the Surf Zone Mine Counter Measures technology programs.

Approved by:

MARY E LACEY, Acting Head
Systems Research & Technology Department

CONTENTS

ILLUSTRATIONS

ILLUSTRATIONS (CONTINUED)

TABLES

CHAPTER 1
INTRODUCTION

The P-α equation of state was original proposed by Herrman[1] to model porous material. This equation of state assumes that a porous material will initially behave elastically when a stress is applied. As the stress is increased, the pores in the material start to crushed, which is an irreversible phenomenon and leads to plastic compression. Unloading of the partially crushed porous material follows a new, elastic curve that depends on the maximum stress achieved by the material. At sufficiently high stress, all pores are eliminated, and the equation of state behavior is that of the original solid material. This P-α model has been used in its original form in the WONDY code[2] and a modified version of it has been included in the CTH code[3]. This modification was proposed by Carroll and Holt[4] and is designed to improve the consistency of the P-α model.

Although the purpose of the P-α equation of state is to treat porous material, the focus in this report is sand. Sand consists of sand grains, water and air or void. This last component will be absent if the sand is fully saturated. However, in most natural situations this will not be the case. The solid part of the P-α model represents the sand grain-water mixture, while the porous part accounts for the air-void content.

It is well known that sand supports a shear stress and several Effective Stress Models have been formulated to represent this characteristic.[5] Although the P-α equation of state cannot directly treat this phenomenon, the shear strength of sand can be addressed by the application of a deviatoric stress model in conjunction with the P-α equation of state.

The Mie-Grueneisen equation of state is used to model the solid state associated with the P-α model. Chapter 2 outlines the Mie-Grueneisen model and its incorporation into DYSMAS. Chapter 3 discusses the P-α equation of state and its implementation while Chapter 4 presents numerical examples. A summary of the report is provided in Chapter 5.

CHAPTER 2
MIE-GRUENEISEN EQUATION OF STATE

The form of the Mie-Gruneisen equation of state described in Reference 3 has been employed.

EQUATION

The Mie-Gruneisen equation of state provides p as a function of ρ and e. The basic form is:

$$p = p_r(\rho) + \Gamma_o \rho_o (e - e_r(\rho)) \tag{1}$$

where $\Gamma = \frac{1}{\rho}\frac{\partial p}{\partial e}$ and $\Gamma\rho = \Gamma_o\rho_o$. The subscript r refers to the reference state which is an isentrope passing through the reference point (p_o, ρ_o, e_o). The reference state is defined by:

$$e_r = e_o + \mu\frac{p_o}{\rho_o} + \frac{c_s^2\mu^2 Y}{2(1-S\mu)} \tag{2}$$

$$p_r = p_o + \frac{\rho_o c_s^2 \mu}{2(1-S\mu)}\left(Y + \mu\frac{dY}{d\mu} + \frac{Y}{(1-S\mu)}\right). \tag{3}$$

Here:

$$\mu = 1 - \frac{\rho_o}{\rho} \tag{4}$$

and

$$Y(\mu) = \sum_{k=0}^{5} a_k \mu^k. \tag{5}$$

The a_k coefficients are defined by:

$$a_0 = 1;\ a_1 = \frac{S}{3};\ a_k = \frac{1}{k+2}[(\Gamma_o + kS)a_{k-1} - \Gamma_o S a_{k-2}] \tag{6}$$

where S is the coefficient relating shock velocity and particle velocity and Γ_o is the Grueneisen parameter at the initial density ρ_o. Note the definition of p_r follows from e_r via:

$$\frac{p_r}{\rho^2} = \frac{de_r}{d\rho} \tag{7}$$

since the reference state is isentropic.

SOUND SPEED

An additional variable required by DYSMAS is sound speed. This is derived as follows:

$$c^2 = \left(\frac{\partial p(\rho, e)}{\partial \rho}\right)_s ,$$
$$c^2 = \left(\frac{\partial p}{\partial \rho}\right)_e \left(\frac{\partial \rho}{\partial \rho}\right)_s + \left(\frac{\partial p}{\partial e}\right)_\rho \left(\frac{\partial e}{\partial \rho}\right)_s , \tag{8}$$
$$c^2 = \left(\frac{\partial p}{\partial \rho}\right)_e + \left(\frac{\partial p}{\partial e}\right)_\rho \frac{p}{\rho^2} .$$

Using Equations (1) and (7) :

$$\left(\frac{\partial p}{\partial e}\right)_\rho = \Gamma_o \rho_o , \tag{9}$$

$$\left(\frac{\partial p}{\partial \rho}\right)_e = \frac{dp_r}{d\rho} - \frac{\Gamma_o \rho_o}{\rho^2} p_r \tag{10}$$

Substituting these definitions into Equation (8) yields the expression for sound speed:

$$c^2 = \frac{dp_r}{d\rho} + \frac{\Gamma_o \rho_o}{\rho^2}(p - p_r) . \tag{11}$$

To evaluate c^2 it is necessary to compute $dp_r/d\rho$. Differentiating Equation (3) produces:

$$\frac{dp_r}{d\rho} = \frac{\rho_o}{\rho}\frac{dp_r}{d\mu} = \frac{\rho_o^2 c_s^2}{2(1 - S\mu)\rho^2}\left[\frac{2Y}{(1 - S\mu)^2} + \frac{2\mu(2 - S\mu)}{(1 - S\mu)}\frac{dY}{d\mu} + \mu^2 \frac{d^2Y}{d\mu^2}\right] . \tag{12}$$

Rearranging Equation (11) and substituting Equation (10) yields an additional relation which is applied in the DYSMAS equation of state routines is:

$$\left(\frac{\partial p}{\partial \rho}\right)_e = \left[c^2 - \frac{\Gamma_o \rho_o p}{\rho^2}\right] . \tag{13}$$

CHANGES OF STATE

The DYSMAS code requires isentropic and Hugoniot changes of state calculations: given an initial state (ρ_1, e_1) and a second density, ρ_2, compute the corresponding energy e_2 which is on the original isentrope or Hugoniot.

For an isentropic process

$$de = \frac{p\,d\rho}{\rho^2} = \left[\frac{p_r}{\rho^2} + \frac{\Gamma_o \rho_o}{\rho^2}(e - e_r)\right] d\rho \tag{14}$$

Since the reference state is isentropic,

$$de_r = \frac{p_r}{\rho^2} d\rho \tag{15}$$

Equation (14) reduces to:

$$\frac{d(e - e_r)}{(e - e_r)} = \Gamma_o \rho_o \frac{d\rho}{\rho^2} \tag{16}$$

Integrating this equation produces the isentropic change of state formula.

$$e_2 = e_r(\rho_2) + [e_1 - e_r(\rho_1)] exp\left(\frac{\Gamma_o \rho_o (\rho_2 - \rho_1)}{\rho_2 \rho_1}\right). \tag{17}$$

The Hugoniot change of state relation follows directly from the Hugoniot condition

$$p_1 + p_2 = \frac{2\rho_1 \rho_2 (e_2 - e_1)}{(\rho_2 - \rho_1)}\,. \tag{18}$$

Eliminating e from this equation via Equation (1) and solving for p_2 produces

$$p_2 = p_1 + \frac{\rho_1 \rho_2 C - p_1(\rho_2 - \rho_1)}{\frac{(\rho_2 - \rho_1)}{2} - \frac{\rho_1 \rho_2}{\Gamma_o \rho_o}}\,, \tag{19}$$

where:

$$C = \left\{ e_r(\rho_2) - e_r(\rho_1) + \frac{[p_r(\rho_2) - p_r(\rho_1)]}{\Gamma_o \rho_o} \right\}$$

DELTA FORMULATION

For compatibility with the DYSMAS code, Equation (1) is written in delta form which references pressure, density, and energy to an ambient state $(p_\infty, \rho_\infty, e_\infty)$. Each material has its own density and energy ambient state, while a common ambient pressure is used for all materials. This leads to the following definitions for the delta variables:

$$\begin{aligned} \Delta p &= p - p_\infty \\ \Delta p_r &= p_r - p_\infty \\ \Delta e &= e - e_\infty \\ \Delta e_r &= e_r - e_\infty \\ \Delta \rho &= \rho - \rho_\infty \end{aligned} \tag{21}$$

Recasting μ in delta form produces

$$\mu = \frac{\Delta \rho}{\rho} + \frac{(\rho_\infty - \rho_o)}{\rho} \,. \tag{22}$$

The delta form diminishes the truncation error in expressions which contain the difference between to state variables. This issue is of concern since DYSMAS is a single precision code. The equations necessary to implement the Mie-Grueneisen equation of state in DYSMAS are re-cast as follows:

$$Eq.\,(1): \quad \Delta p = \Delta p_r + \Gamma_o \rho_o [\Delta e - \Delta e_r] \,, \tag{23}$$

$$Eq.\,(11): \quad c^2 = \frac{dp_r}{d\rho} + \frac{\Gamma_o \rho_o}{\rho^2}(\Delta p - \Delta p_r) \,, \tag{24}$$

$$Eq.\,(13): \quad \left(\frac{\partial \Delta p}{\partial \Delta \rho}\right)_e = \left[c^2 - \frac{\Gamma_o \rho_o (\Delta p_r + p_\infty)}{\rho^2}\right] \,, \tag{25}$$

$$Eq.\,(17): \quad \Delta e_2 = \Delta e_r(\rho_2) + [\Delta e_1 - \Delta e_r(\rho_1)] exp\left(\frac{\Gamma_o \rho_o (\Delta \rho_2 - \Delta \rho_1)}{\rho_1 \rho_2}\right) \,, \tag{26}$$

$$Eq.\,(19): \quad \delta p = \frac{\rho_1 \rho_2 C - p_1(\Delta \rho_2 - \Delta \rho_1)}{\frac{\delta \rho}{2} - \frac{\rho_1 \rho_2}{\Gamma_o \rho_o}}; \; C = \delta e_r + \frac{(\Delta p_{r_2} - \Delta p_{r_1})}{\Gamma_o \rho_o} \,. \tag{27}$$

DYSMAS IMPLEMENTATION

The DYSMAS code requires equation of state routines which perform the 6 different functions listed below:

- Function f_1: Compute $\Delta p_1, c_1^2$ given $\Delta\rho_1, \Delta e_1$,
- Function f_2: Compute $\Delta p_2, \Delta e_2, c_2^2$ given $\Delta\rho_1, \Delta e_1, \Delta\rho_2$ and assuming an isentropic change of state between $\Delta\rho_1$ and $\Delta\rho_2$,
- Function f_3: Compute $\Delta p_2, \Delta e_2, c_2^2$ given $\Delta\rho_1, \Delta e_1, \Delta\rho_2$ and assuming a change of state along the Hugoniot between $\Delta\rho_1$ and $\Delta\rho_2$,
- Function f_4: Compute $\Delta\rho_1, c_1^2$ given $\Delta p_1, \Delta e_1$,
- Function f_5: Compute $\Delta\rho_2, \Delta e_2, c_2^2$ given $\Delta p_1, \Delta e_1, \Delta p_2$ and assuming an isentropic change of state between Δp_1 and Δp_2,
- Function f_6: Compute $\Delta\rho_2, \Delta e_2, c_2^2$ given $\Delta p_1, \Delta e_1, \Delta p_2$ and assuming a change of state along the Hugoniot state between Δp_1 and Δp_2.

A description of these subroutines is provided in Appendix A.

CHAPTER 3
P-α EQUATION OF STATE

DESCRIPTION

The basic form of the P-α equation is:

$$p = p(\alpha,\rho,e) = \frac{p_s(\alpha\rho,e)}{\alpha} \tag{28}$$

where

$$\alpha = \frac{\rho_s}{\rho}\,. \tag{29}$$

Here the subscript s denotes properties of the underlying solid material and the variables that are not subscripted pertain to the porous media. The condition of the porous media is dictated by the function

$$\alpha = A(p, p_t, p_{max}) \tag{30}$$

which is sketched in Figure 1 and has multiple elastic branches. Here p_t is the material derivative of p; positive values indicate loading, while negative ones indicate unloading. p_{max} is the maximum pressure that has been sustained by the material. This parameter follows the fluid and is used to select the appropriate branch of the elastic curve.

For values of $\alpha > 1$, the porous material sound speed is defined as a linear function of porosity:

$$c = c_s + (c_e - c_s)\frac{(\alpha - 1)}{(\alpha_o - 1)}\,. \tag{31}$$

When $\alpha = 1$, c is computed from the Mie-Grueneisen relations. Here c_s and c_e are the reference speeds of sound in the fully dense solid and virgin materials.

ELASTIC AND PLASTIC α RELATIONS

As shown in Figure 1, the function A has multiple branches and features an unloaded (virgin) value of $\alpha=\alpha_o$. The appropriate branch of A is selected as follows:

1. When loaded, the virgin material compresses elastically along curve A^a_{el} until a pressure of p_e is reached (i.e. point A).
2. In response to further loading, the plastic curve A_{pl} is followed until the pressure reaches p_s. Here α=1, a value which is retained forever.
3. The unloading path followed from a point on the plastic curve, is along the intersecting elastic curve. For example, point B unloads along A^b_{el}.
4. From a position on an elastic curve, the loading path follows the elastic curve until the plastic curve is reached. Further loading is along the plastic curve.

The above description of p-α material behavior indicates that a state (p, p_{max}, p_t) is on the plastic curve if $p_t \geq 0$ and $\alpha = A_{pl}(p)$; otherwise it is on the elastic curve which intersects the plastic curve at p_{max}. Noting that A is a monotone function of p, it is possible to simplify this rule: a state is on the plastic curve if $p \geq p_{max}$ and on the elastic curve otherwise.

Alternatively, it is possible to cast the test for the plastic curve location in terms of α: a state is on the plastic curve if $\alpha \leq \alpha_{min}$ and otherwise on the elastic curve intersecting α_{min}. Here α_{min} is the minimum value of α attained by the material in the cell. Since it is a historical marker, it must be convected with the fluid and it is initialized by setting $\alpha_{min} = \alpha_e$. This rule can be expressed:

$$\alpha = A(p, \alpha_{min}) = \begin{cases} A_{pl}(p) & if\ A_{pl}(p) \leq \alpha_{min} \\ A_{el}(p, \alpha_{min}) & otherwise \end{cases} \tag{32}$$

Inverting A, as is shown in Figure 2, and solving for p yields:

$$p = P(\alpha, \alpha_{min}) = \begin{cases} P_{pl}(\alpha) & if\ \alpha \leq \alpha_{min} \\ P_{el}(\alpha, \alpha_{min}) & otherwise \end{cases} \tag{33}$$

The equation for the plastic curve is:

$$A_{pl}(p) = 1 + (\alpha_e - 1)\left(\frac{p_S - p}{p_S - p_e}\right)^2, \tag{34}$$

which can also be inverted to obtain:

$$P_{pl}(\alpha) = p_S - (p_S - p_e)\left[\frac{(\alpha - 1)}{(\alpha_e - 1)}\right]^{\frac{1}{2}}. \tag{35}$$

Traditionally, the elastic curve, $\overline{A}_{el}$, is given in the differential form

$$\frac{d\overline{A}_{el}(\alpha)}{dp} = \frac{\alpha^2}{K_c}\left(1 - \frac{1}{h^2}\right);\ h = 1 + \frac{(c_e - c_s)(\alpha - 1)}{c_s(\alpha_o - 1)}, \tag{36}$$

where K_c is the bulk modulus $(\rho_s c_s^2)$ of the solid material. In the present work, this differential relation has been replaced by a linear one:

$$A_{el}(p, \alpha_{min}) = \alpha_{min} + \frac{d\overline{A}_{el}(\alpha_{min})}{dp}(p - P_{pl}(\alpha_{min})) \tag{37}$$

The significance of this change can be appreciated by constructing the P-α elastic-plastic curves from Equations (34) and (36) for parameter values typical of sand. Results are shown in Figure 3 and indicate that the elastic curves are nearly linear except as $\alpha \rightarrow \alpha_o$ where the elastic curves displays a nonlinear behavior, rising above the plastic curve, A_{pl} .

. Inverting Equation (37) and solving for p yields:

$$P_{el}(\alpha, \alpha_{min}) = P_{pl}(\alpha_{min}) + \left(\frac{\alpha - \alpha_{min}}{\frac{d\overline{A}_{el}(\alpha_{min})}{dp}}\right). \tag{38}$$

COMPUTING p AND ρ

The strategy for implementing the P-α model in DYSMAS is to make this it appear similar to a conventional equation of state. All the work needed to support this equation of state is encapsulated within a single routine that is called as a function of ρ,e and $\alpha_{\min}$. This is accomplished by equating Equations (28) and (33) and iteratively solving the resulting nonlinear relation

$$p(\alpha, \rho, e) = P(\alpha, \alpha_{min}) \tag{39}$$

for α.

The solution of Equation (39) requires the selection of the appropriate branch of the $P(\alpha, \alpha_{min})$ curve of which there are three possibilities: elastic, plastic, and the α=1 extension for compressed material. These three branches are illustrated in Figure 2 for $\alpha = \alpha'_{min}$. Also shown, are three graphs for Equation (28), each associated with a different solution branch. The graphs for the $p(\alpha, \rho_1, e_1)$, $p(\alpha, \rho_2, e_2)$, *and* $p(\alpha, \rho_3, e_3)$ curves intersects the α=1 line, the plastic curve and the elastic curve, respectively. The iterative procedure first determines the appropriate branch of the P curve and then calculates the point of intersection. The α=1 extension is selected if $p(1, \rho, e) \geq p_s$ *or* $\alpha_{min} = 1$; otherwise the plastic branch applies if $p(\alpha_{min}, \rho, e) > P_{pl}(\alpha_{min}, \alpha_{min})$. If both tests fail, the intersection with the elastic curve $P_{el}(\alpha, \alpha_{min})$ is computed.

The computation of ρ given $\alpha_{\min}$, p, e, is a two step process; compute α from Equation (33) and then use the Mie-Grueneisen function f_4 to determine the value ρ, which satisfies:

$$\alpha p = p_s(\alpha\rho, e) \; . \tag{40}$$

CHANGES OF STATE

The isentropic state change is computed by integrating

$$e_2 = e_1 + \int_{\rho_1}^{\rho_2} \frac{p}{\rho^2} d\rho \; . \tag{41}$$

For a P-α material, a closed-form solution is not available and this equation must be solved numerically. To improve efficiency, the numerical integration need only be carried out when $\alpha > 1$. The remaining part of the integration can be computed from the Mie-Grueneisen equation of state relation, Equation (17).

Hugoniot changes of state are computed by solving the Hugoniot condition:

$$p_1 + p_2 = \frac{2\rho_1\rho_2(e_2 - e_1)}{(\rho_2 - \rho_1)} \; . \tag{42}$$

If α_1 and α_2 are known, Equation (42) can be written in terms of the solid Mie-Grueneisen properties (ρ_s, p_s) and e can be eliminated. Reintroducing the porous material properties yields:

$$p_2 = p_1 + \frac{C_1\rho_1\rho_2 - p_1 C_2}{\frac{(\rho_2-\rho_1)}{2} - \frac{\rho_1\rho_2\alpha}{\Gamma_o\rho_o}} . \tag{43}$$

where:

$$\begin{aligned} C_1 &= e_r(\alpha_2\rho_2) - e_r(\alpha_1\rho_1) - \frac{[p_r(\alpha_2\rho_2) - p(\alpha_1\rho_1)]}{\Gamma_o\rho_o} \\ C_2 &= (\rho_2 - \rho_1) - \frac{\rho_2\rho_1(\alpha_2 - \alpha_1)}{\Gamma_o\rho_o} \end{aligned} \tag{44}$$

With p_2 known, e_2 follows from:

$$e_2 = e_r(\alpha_2, \rho_2) + \frac{[\alpha_2 p_2 - p_r(\alpha_2, \rho_2)]}{\Gamma_o\rho_o} \tag{45}$$

Since α_2 is often not known, it may be necessary to imbed these relations in an iterative procedure.

DYSMAS IMPLEMENTATION

A necessary consideration in coupling the P-α equation of state to DYSMAS is compatibility with the delta formulation. The solid state regime of the P-α equation of state is much stiffer than the porous one, and consequently, there is a greater need for accuracy here. Hence the solid density and energy reference states are used to normalize the density and energy and the following definitions apply:

$$\begin{aligned} \Delta p &= p - p_\infty; \quad \Delta p_s = p_s - p_\infty \\ \Delta\rho &= \rho - \rho_\infty; \; \Delta\rho_s = \rho_s - \rho_\infty \\ \Delta e &= e - e_\infty; \; \Delta e_s = e_s - \rho_\infty \end{aligned} \tag{46}$$

Substituting the above into Equations (28) and (29) yields the following relations between solid and porous material delta properties:

$$\begin{aligned} \Delta p_s &= \Delta p + p_\infty(\alpha - 1) \\ \Delta e_s &= \Delta e \\ \Delta\rho_s &= \Delta\rho + \rho_\infty(\alpha - 1) . \end{aligned} \tag{47}$$

The required DYSMAS P-α equation of state functions are as follows:

- Function F_1: Compute $\Delta p_1, c_1^2, \alpha_1$ given $\Delta\rho_1, \Delta e_1, \alpha_{min}$.
- Function F_2: Compute $\Delta p_2, \Delta e_2, c_2^2, \alpha_2$ given $\Delta\rho_1, \Delta e_1, \Delta\rho_2, \alpha_{min}$ and assuming an isentropic change of state between $\Delta\rho_1$ and $\Delta\rho_2$.
- Function F_3: Compute $\Delta p_2, \Delta e_2, c_2^2, \alpha$ given $\Delta\rho_1, \Delta e_1, \Delta\rho_2, \alpha_{min}$ and assuming a change of state along the Hugoniot between $\Delta\rho_1$ and $\Delta\rho_2$.
- Function F_4: Compute$\Delta\rho_1, c_1^2, \alpha_1$ given $\Delta p_1, \Delta e_1, \alpha_{min}$
- Function F_5: Compute $\Delta\rho_2, \Delta e_2, c_2^2, \alpha_2$ given $\Delta p_1, \Delta e_1, \Delta p_2, \alpha_{min}$ and assuming an isentropic change of state between Δp_1 and Δp_2.
- Function F_6: Compute $\Delta\rho_2, \Delta e_2, c_2^2, \alpha_2$ given $\Delta p_1, \Delta e_1, \Delta p_2, \alpha_{min}$ and assuming a change of state along the Hugoniot between Δp_1 and Δp_2.

A detailed description of these routines is provided in Appendix B

The interaction between the DYSMAS scheme and the P-α equation of state during a computational step can be summarized as follows:

- In phase 1, calculated c from Equation (33) with α=α_l. Here α_l is the value of α computed in the previous cycle.
- Execute the standard Euler algorithm, phases 1–5. However, add the convection of $\alpha_{\min}$ using:

$$\frac{\partial(\rho\alpha_{min})}{\partial t} + \mathbf{V}\cdot\nabla(\rho\alpha_{min}) = 0 \tag{48}$$

- Use the convected value of $\alpha_{\min}$ in phase 6 to service equation of state calls which then return the new value of α=α_l
- At the end of Phase 6, for each cell define:

$$\alpha_{min} = min(\alpha_l, \alpha_{min}) \tag{49}$$

CHAPTER 4
NUMERICAL RESULTS

The numerical scheme outlined in the preceding section has been applied to several types of cases. The first type is designed to validate implementation of the P-α and compares DYSMAS to exact solutions and other codes containing the P-α model. The second type tests the ability of the P-α equation of state to simulate sand. This is accomplished by comparing calculation and experiment.

VALIDATION TESTS

The implementation of the P-α model in DYSMAS is tested by comparing with an exact Riemann solution as well as with the CTH[4] and MMG[6] codes. The Mie-Grueneisen and P-α parameters used in the verification tests are listed in Table 1.

QUANTITY	Verification Tests	SRI 100%	SRI 95%	SRI 78%.	SAMSI
S	1.93	2.17	2.18	2.13	2.2
c_s	$.148(10^6)$	$.2(10^6)$	$.2(10^6)$	$.2(10^6)$	$.14(10^6)$
ρ_o	2.070	2.052	2.052	2.012	1.444
Γ_o	.880	.865	.870	.846	.610
α_o	1.052364	N/A	1.01988	1.10854	1.00958
ps	$6.5(10^7)$	N/A	$5.(10^9)$	$5.(10^9)$	$.138(10^8)$
c_e	$6.0(10^4)$	N/A	$6.0(10^4)$	$6.0(10^4)$	$1.13(10^4)$
p_e	0.	N/A	0.	0.	0.
α_e	1.052364	N/A	1.01988	1.10854	1.00958

TABLE 1. MIE-GRUENEISEN AND P-α PARAMETERS FOR TEST CASES.

Riemann Problem Solutions

Solutions for fully saturated sand and partially saturated sand are considered. Fully saturated sand is represented by the Mie-Grueneisen Equation of state while the P-α Equation of state is used to model the partially saturated sand. Computed densities for these two cases are shown in Figures 4 and 5 and close agreement between computation and experiment is achieved. These calculations were run using 500 mesh points. The left and right states for

the fully saturated case were: $\rho_l = 2.20, e_l = 5(10^5), p_l = 4.69(10^9)$; $\rho_r = 2.054, e_r = 5(10^8), p_r = 4.42(10^7)$ $u_r = 0$. The conditions for the partially saturated case were: $p_l = 4.23(10^9), \rho_l = 2.20, e_l = 5(10^8)$; $p_r = 4.42(10^7), \rho_r = 1.97, e_r = 5(10^5)$. In both cases, left and right state velocities were initially zero.

1–D Spherical bubble for Fully Saturated Sand

This problem consists of a spherical, high pressure gas bubble containing a gamma law gas (γ = 1.3) imbedded in fully saturated sand. The sand is described with a Mie-Grueneisen equation of state and the computation was completed using a CFL number of .8. The computed spatial pressure and velocity profiles are exhibited for the DYSMAS, CTH, and MMG codes in Figures 6 and 7 at five different times during the calculation. The results from both codes are in good agreement except inside the bubble, where the velocities differ. Temporal plots of the velocity at points within the bubble exhibit rapid oscillation in all three of the codes, reflecting the repeated reflection of shock and expansion waves across the bubble, in response to the bubble surface motion. To the extent that the bubble surface does not move in precisely the same way in each code, the velocities within the bubble differ.

1–D Spherical bubble for Partially Saturated Sand

This cases is similar to the preceding one with the exception that the sand is not fully saturated. Accordingly, the sand was modeled using a P-α equation of state with α_o taken to be 1.052808. The computation was completed using a CFL number of .45 and FCT diffusion and antidiffusion values of .125.

The computed spatial pressure, velocity and α profiles are shown at four different times using the DYSMAS, CTH and MMG codes in Figures 8, 9 and 10. As in the fully saturated sand case, pressure agrees well everywhere, while the velocities are in good agreement within the sand. The α values are also in close agreement everywhere. Figures 11 and 12 provide the pressure and velocity time histories at three different locations near the explosion bubbles. These figures compare the DYSMAS, MMG, and CTH codes and close agreement is obtained.

Figures 13 and 14 demonstrate the influence of the FCT diffusion and antidiffusion parameters (FCTDIF and FCTADF) on the spatial pressure and velocity distribution. Each of these figures exhibits calculations with FCTDIF=FCTADF=.125 and FCTDIF=FCTADF=.5. Changes in the FCT parameters influence the pressure near the shock and near the bubble. Increasing FCT values widened the compute front and decreased the pressure near the bubble surface.

2–D TNT Explosion

The computational domain is shown in Figures 15 and 16 and features partially saturated sand in the lower and water in the upper half of the domain. The initial TNT charge is located on the sand surface. The computation was completed using a CFL number of .45 and FCT parameter settings of .5. The calculation was viable for lower values of the FCT parameters; however, the solutions exhibited excessive oscillations. The pressure distribution is shown in Figure 15 and clearly illustrates the propagation of the explosion shock through the water and sand. The diminished shock radius in the sand along the vertical is a consequence of the lower sound speed in this material. The sand shock shape curves outwards near the water/sand interface. This is a consequence of the pressure imposed on the sand by the shocked water near this interface.

Figure 16 illustrates the behavior of α in the computational domain. The black level is that of the virgin sand (α = 1.052808) while the light level in the water and behind the sand shock represents a value of 1. It is evident that the passage of the shock compresses the sand material to a solid state.

Computed pressure profiles are compared for the DYSMAS and MMG codes in Figures 17, 18 and 19. The first of these figures illustrates the pressure profile along the centerline of the computational domain. The remaining two figures demonstrate horizontal traverses through the flow field, slightly above and slightly below the sand/water interfaces. This three paths are indicated by the dotted lines in Figure 15.

APPLICATION OF P-α TO SAND TESTS

The capability of the P-α equation of state to model sand is tested by comparing with experiment. Two different sets of data are used: SRI 1–D sand explosions and SAMSI 2–D explosive induced deformation of the buried target. In each case, initial estimates of the Mie-Grueneisen equation of state parameters were constructed from the water and sand grain value as described in Appendix E. Additional p-α parameters were based on test results (if available) and experimentation.

SRI Particle Velocity Tests

The SRI tests consist of an explosion within a sand filled, cylindrical container[7]. Particle velocities at different distance from the explosion were measured as a function of time. The resulting experiment is 1–D until the shock arrives at the container walls. Measurements were made using fully saturated, 95% saturated and 78% saturated sand.

The Mie-Grueneisen parameters (c_s, S, and Γ_o) for the fully saturated sand-water mixture were adjusted to best match experiment. The initial density was available from the experiment. For partially saturated sand, additional parameters need to be specified: α_o, p_S, and p_e. α_o was computed from the measured dry, fully saturated and partially saturated sand density, p_e was taken as zero and P_s was adjusted to best match experiment. The selected set of parameters is given in Table 1.

The measured results for the SRI test are shown in Figures 20, 21 and 22 along with the computational results for each test. An examination of these figures indicates that the computed velocity immediately following the arrival of the explosion shock are in reasonable agreement with experiment. However, experimental results diminish faster than the calculated results.

SAMSI Target Deformation Tests Conducted At WES

In each of these three tests[8], a mine-like target was buried in a sand-like soil and subjected to an explosive shock. The experimental arrangement for this test is depicted in Figure 23a and features 8 lbs of pentolite and an 8in in diameter aluminum target. Pressures were monitored at several locations in the sand and the final deformation of the mine face was recorded.

The first SAMSI test has been simulated with a coupled Eulerian/Lagrangian DYSMAS calculation. The setup for this calculation, including the grids for the Euler and Lagrangian modules, are depicted in Figure 23b. The calculation was performed using 2–D, cylindrical coordinates, with the coordinate axis orientated along the center of the explosive charge and the mine. The water above the sand and the *in-situ* soil, located 3 ft below the mine were ignored.

The "sand" in this test consisted of a grout with a nominally .5% to 1% air content. Density was the only piece of information available to characterize the sand. The remainder of the P-α equation of state parameters were determined empirically by comparing calculation and sand pressure measurements. Table 1 provides the selected set of parameter values.

The evolution of the flow field is shown in Figures 24 to 27. Here the passage of the shock through the sand is clearly visible as is the interaction between the shock and the deforming target surface. The weak shock visible in Figure 26 above the cylinder arises from the initial impact shock transmitted through the target. A comparison of the measured and the calculated pressures in the sand is provided in Figure 28. The calculations are in reasonable agreement with experiment, although the computed pressure level is marginally higher than experiment for the gauge near to the explosion.

Figure 29 presents the displacement history at the target surface centerline. Also included in this figure is the target translation and a second curve which is the difference between the displacement and the translation. This final curve represents the centerline deformation The final computed target-surface deformation profile is shown in Figure 30 and is in good agreement with measured values, which are also given.

CHAPTER 5
SUMMARY AND CONCLUSIONS

The Mie-Grueneisen and P-α equations of state have been incorporated into the DYSMAS code. The form of these equations of state follows from Reference 3; however, the manner of implementation has been altered to provided compatibility with the DYSMAS code. In particular, these equations were cast in the DYSMAS delta form and two auxiliary functions were constructed to compute isentropic and Hugoniot jumps. In addition, a second form for these equations of state and auxiliary functions were developed which were a function of (p,e) rather than the usual (ρ,e). The inverted equation of state form and auxiliary function were implemented numerically.

The P-α equation of state routine was constructed to be similar to other equations of state and differs only in the need to specify the minimum α . This parameter represents the minimum value of α attained by the material at the point of interest. Thus, the form for the equation of state is $p(\alpha_{min},\rho,e)$ or $\rho(\alpha_{min},p,e)$. A Newton iteration was performed to determine the pressure or density associated with the calling arguments.

The implementations of the Mie-Grueneisen and P-α equations of states have been numerically verified by comparing with exact solutions and the results from other codes. The exact solutions cases were 1–D planar Riemann problems, while the code comparison cases consisted of a spherical explosion (explosive surround by sand) and a 2–D simulation of an underwater explosive sitting on a sand bottom. In all cases, the DYSMAS results compared closely to the appropriate benchmark.

The veracity of P-α as a sand model was tested by comparing with two experiments. The first was the SRI explosion in a canister test which was simulated using a 1–D spherical calculation. The second test featured a target buried in sand that was subjected to an explosion. In the latter case, the Euler code was coupled to the Lagrangian code, and target deformation as well as sand pressure were compared to experiment. In both cases the predictions and experiment were in reasonable agreement with experiment.

The numerical results presented in this paper establish the validity of the P-α implementation in the DYSMAS code. In addition, agreement between calculation and experiment demonstrated on the two test cases is encouraging. However, additional comparisons with experiment are necessary to more fully ascertain the merits of the P-α equation of state as a sand model.

REFERENCES

1. Herrman, W. "Constitutive Equations for the Dynamic Compaction of Ductile Porous Material", **J. of Appl Phys, 40**, 6, May 1969.

2. Kipp, M. E. and Lawrence, R. J., "A ONE-DIMENSIONAL FINITE-DIFFERENCE WAVE PROPAGATION CODE", Sandia National Laboratories, DE82 19807, June 1982.

3. Kerley, G. I., "CTH Equation of State Package: Porosity and Reactive Burn Models", Sandia National Laboratories, SAND92–0553, April 1992.

4. Carroll, M., and Holt, A., "Suggested Modifications of the P-α Model for Porous Materials", **J. of Appl Phys, 43**, 2, February 1972..

5. Simons, A., "Comparison of several Two-Phase Models for Saturated Porous Media", R & D Associates, RDA-TR-0264238903–001, March 1989

6. Wardlaw, A. B, Private Communication, March, 1995.

7. Gefken, P, Florence, A, Sanai, M. "Spherical Waves in Saturated Sand", NAVSWC/MP-95/0, Sept. 1995.

8. Johnson,, J., Rye, K., Tussing, R., " BEAST CALIBRATION TEST — APRIL 1995", Preliminary Data Report, WES, Vicksburg, MS, April 1995.

GLOSSARY

symbol	Definition
$a_0...a_5$.	see Equation (6)
A	α function, Equation (32)
c	Sound speed
c_e	Reference sound speed in porous material
c_s	Reference sound speed in solid (non-porous) material
e	Energy
e_o	Mie-Gruneisen equation of state reference state energy
e_r	Mie-Gruneisen equation of state reference energy
p	Pressure
p_e	Pressure plastic behavior of P-α material is initiated
p_{max}	Maximum pressure experienced experienced by material
p_o	Mie-Gruneisen equation of state reference state pressure
p_r	Mie-Gruneisen equation of state reference pressure
p_s	Solid material pressure
p_S	Pressure at which all pores are crushed
p_t	Material derivative of pressure
P	Inverse of A function, Equation (33)
s	Entropy
S	Coefficient relating shock (u_o) and particle velocity (u_p): $u_s = c_o + Su_p$
Y	See Equation (5)
α	Degree of porosity, see Equation (29)
α_e	Maximum α where A_{pl} is valid
α_l	Local α at a particular cell
α_o	Initial α at p=0
α_{min}	Minimum value of α achieved by material
$\Delta p, \Delta\rho, \Delta e$	See Equation (21)

$\Delta p_r, \Delta e_r$	See Equation (21)
$\Delta p_s, \Delta \rho_s, \Delta e_s$	See Equation (46)
Γ_o	Gruneisen parameter at ρ_o
μ	Equation (4)
ρ	Density
ρ_o	Mie-Gruneisen equation of state reference state density
ρ_s	Solid material density

Subscripts

1, 2	Initial and final equation of state conditions
el	Elastic curve
pl	Plastic curve
s	Isentropic or solid

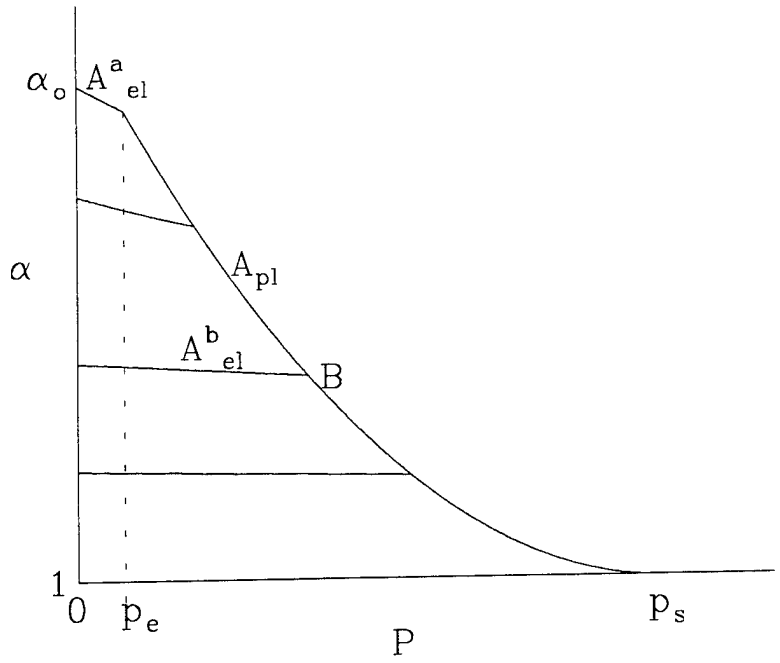

FIGURE 1. P-α ELASTIC AND PLASTIC CURVES

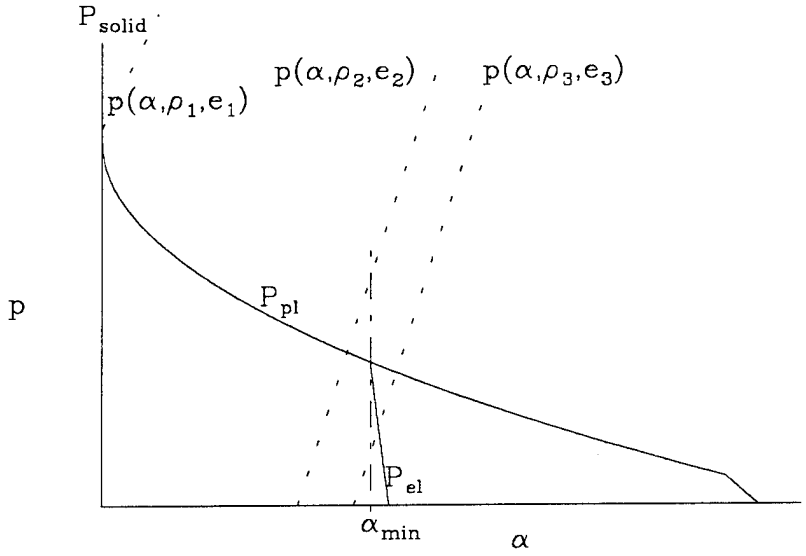

FIGURE 2. POSSIBLE P-α SOLUTIONS OF $p(\alpha, p, e) = P(\alpha_{min}, p)$

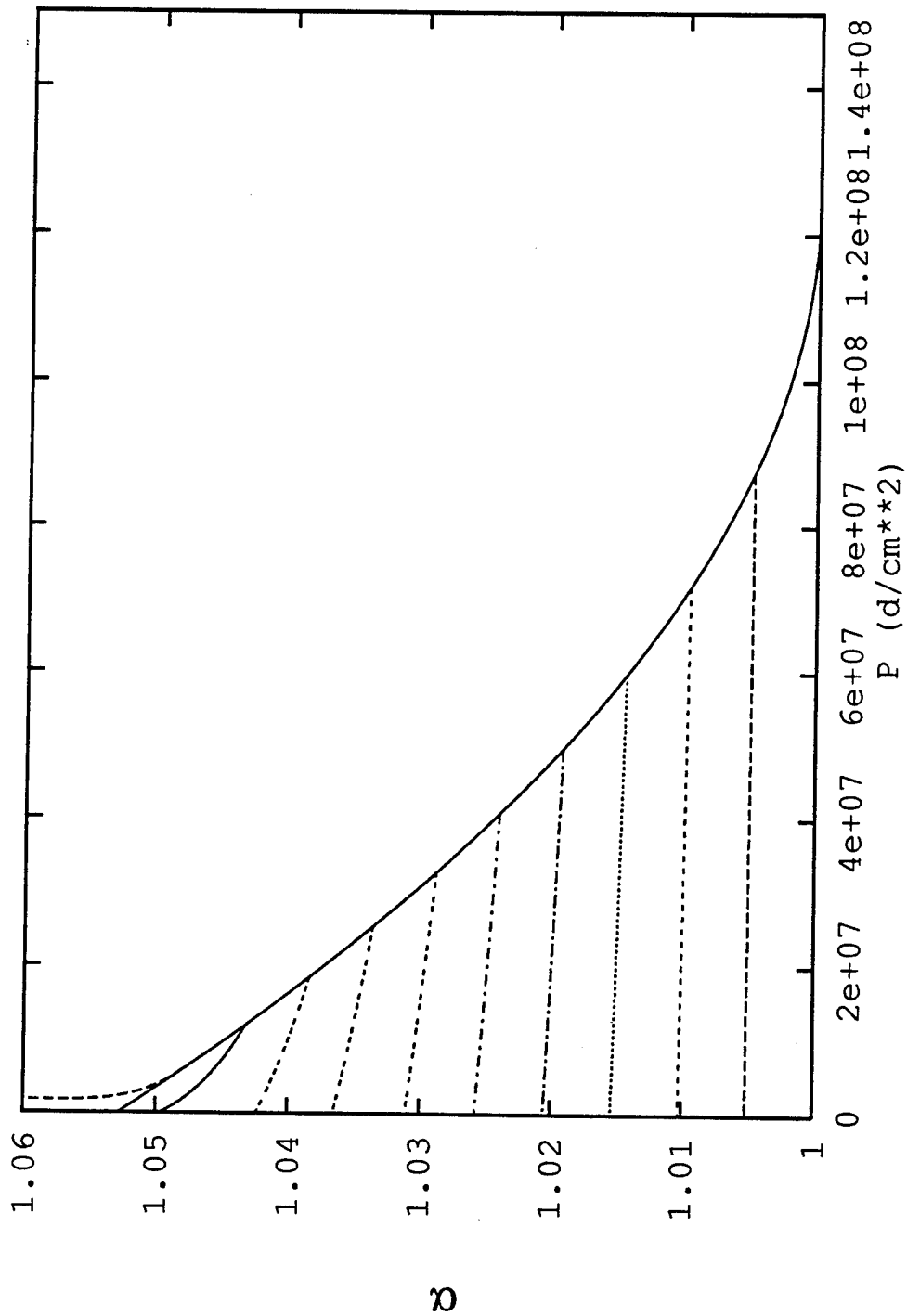

FIGURE 3. NONLINEAR P-α ELASTIC-PLASTIC CURVES FOR A SAND LIKE MATERIAL.

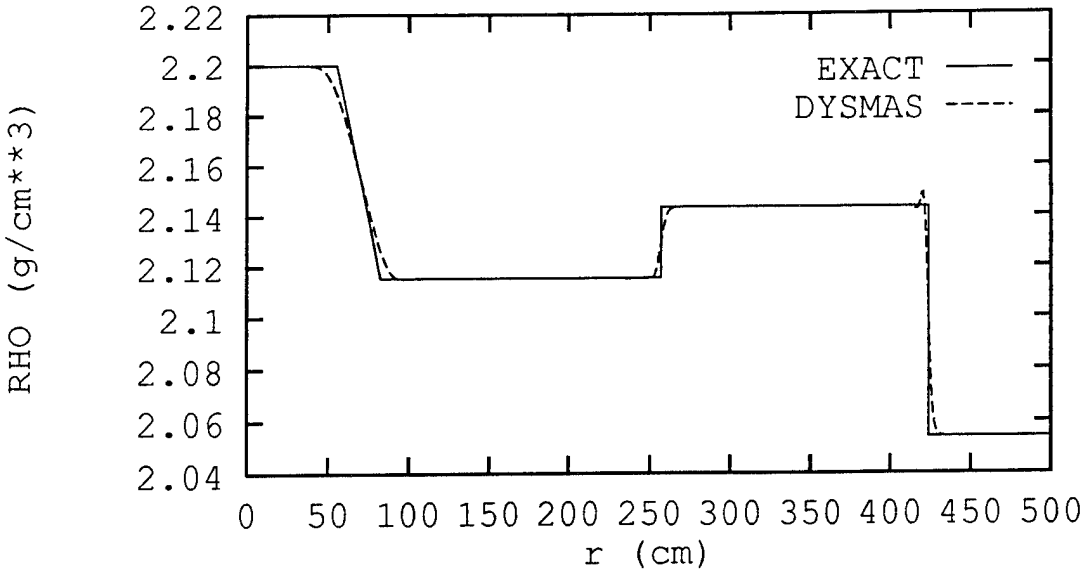

FIGURE 4. COMPUTED AND EXACT DENSITY FOR THE MIE-GRUENEISEN RIEMANN PROBLEM

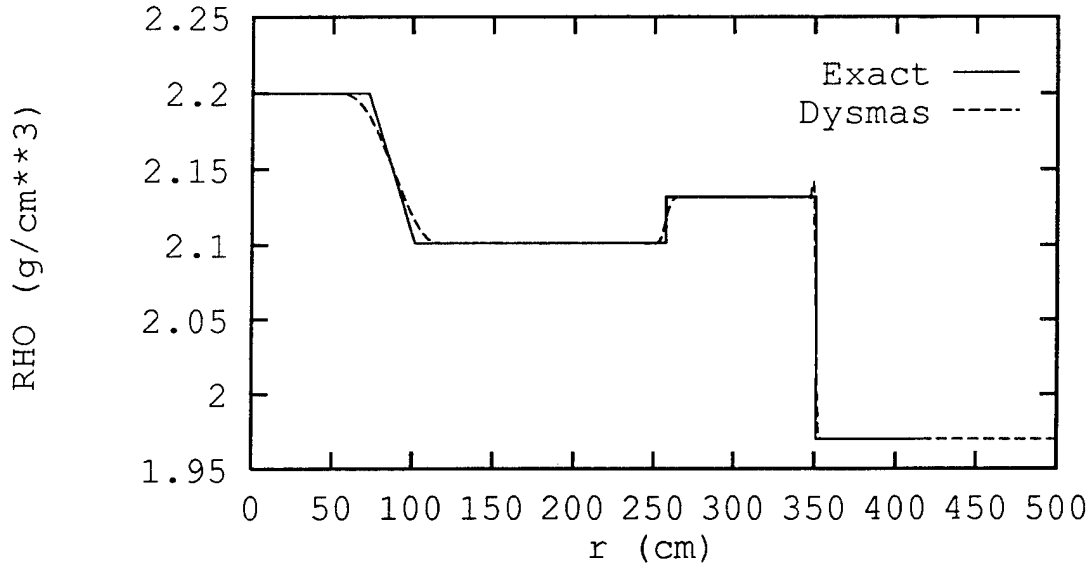

FIGURE 5. COMPUTED AND EXACT DENSITY FOR THE P-α RIEMANN PROBLEM

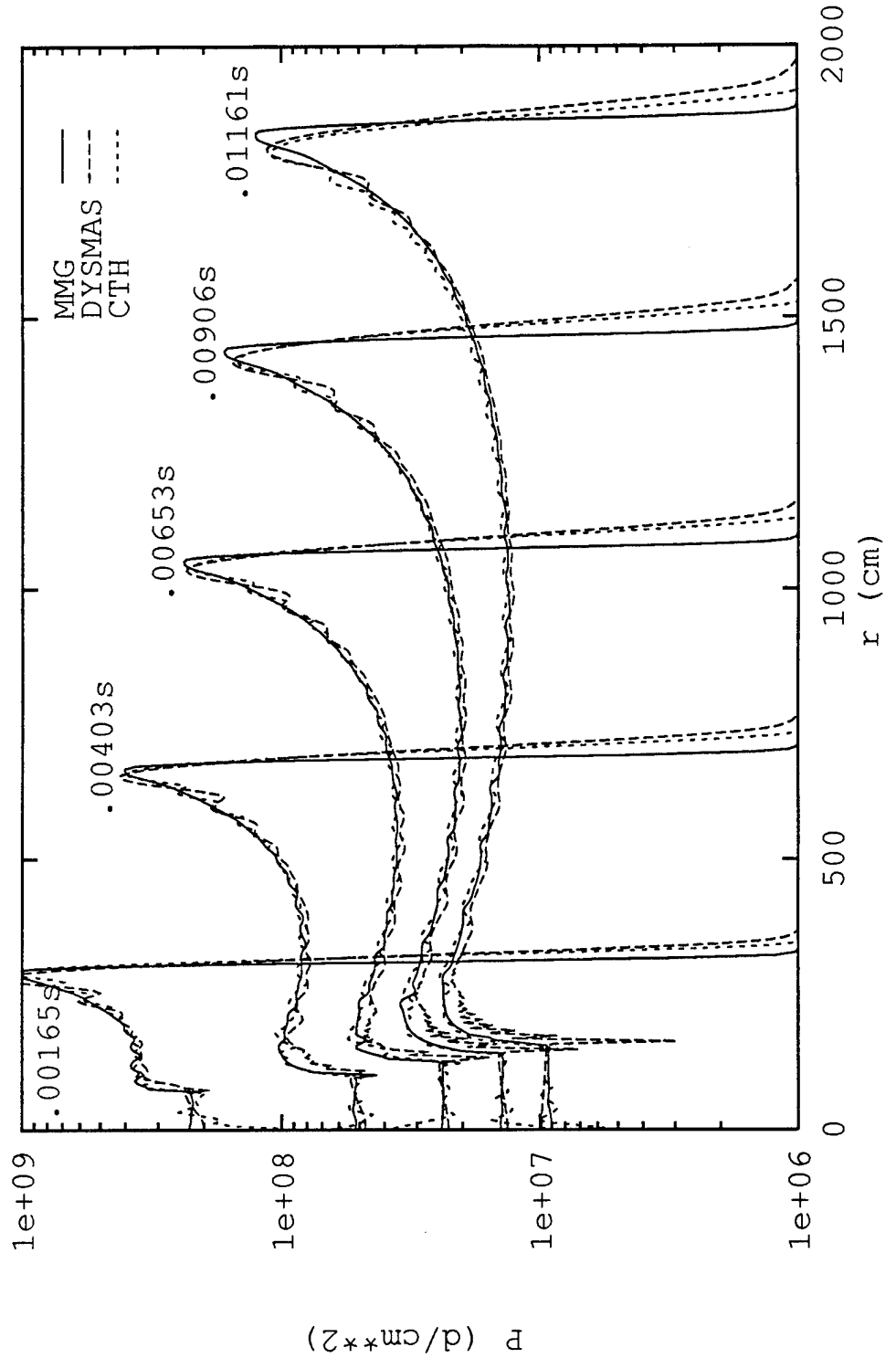

FIGURE 6. PRESSURE RESPONSE OF FULLY SATURATED SAND TO A GAMMA LAW EXPLOSION BUBBLE

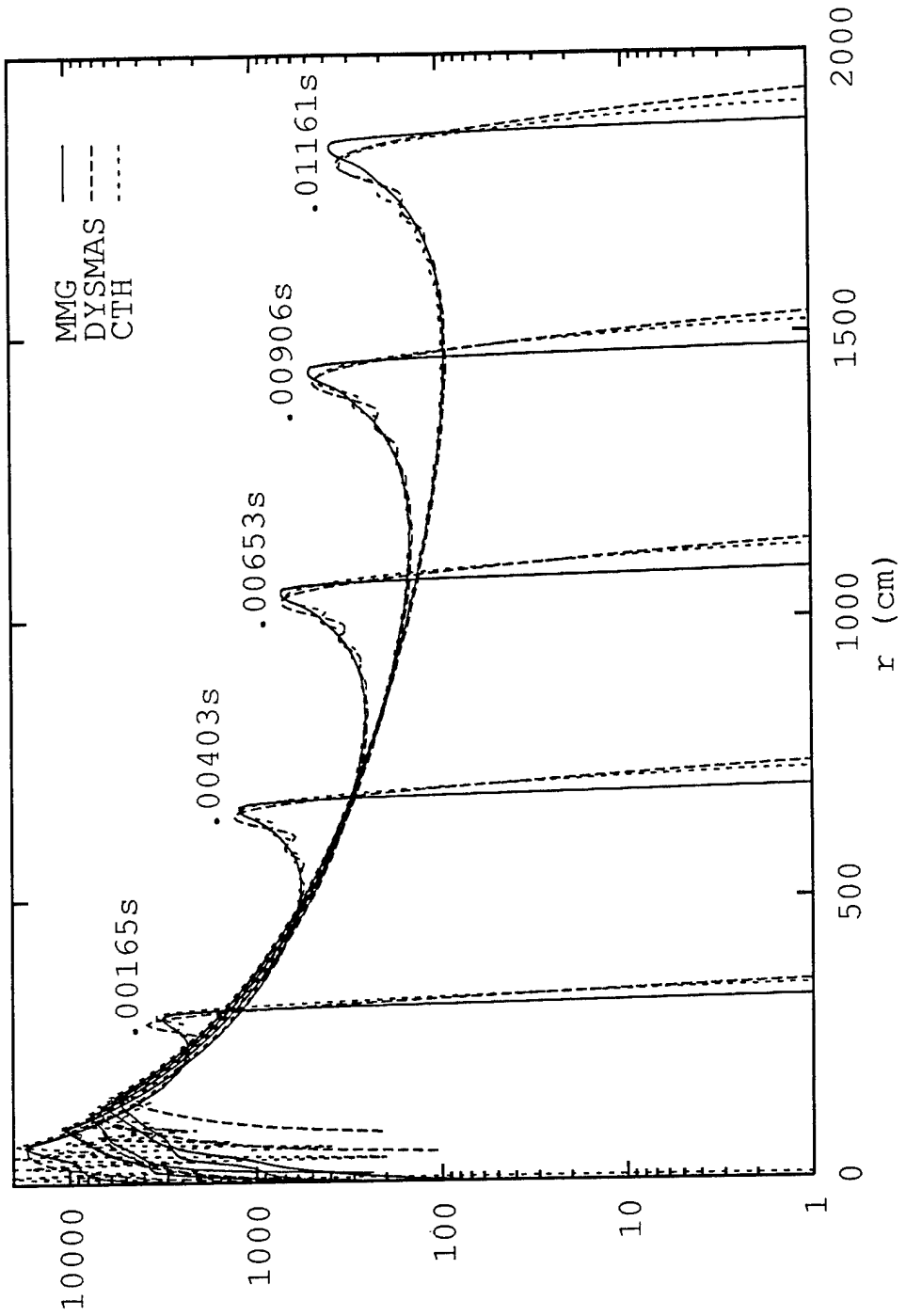

FIGURE 7. VELOCITY RESPONSE OF FULLY SATURATED SAND TO A GAMMA LAW EXPLOSION BUBBLE

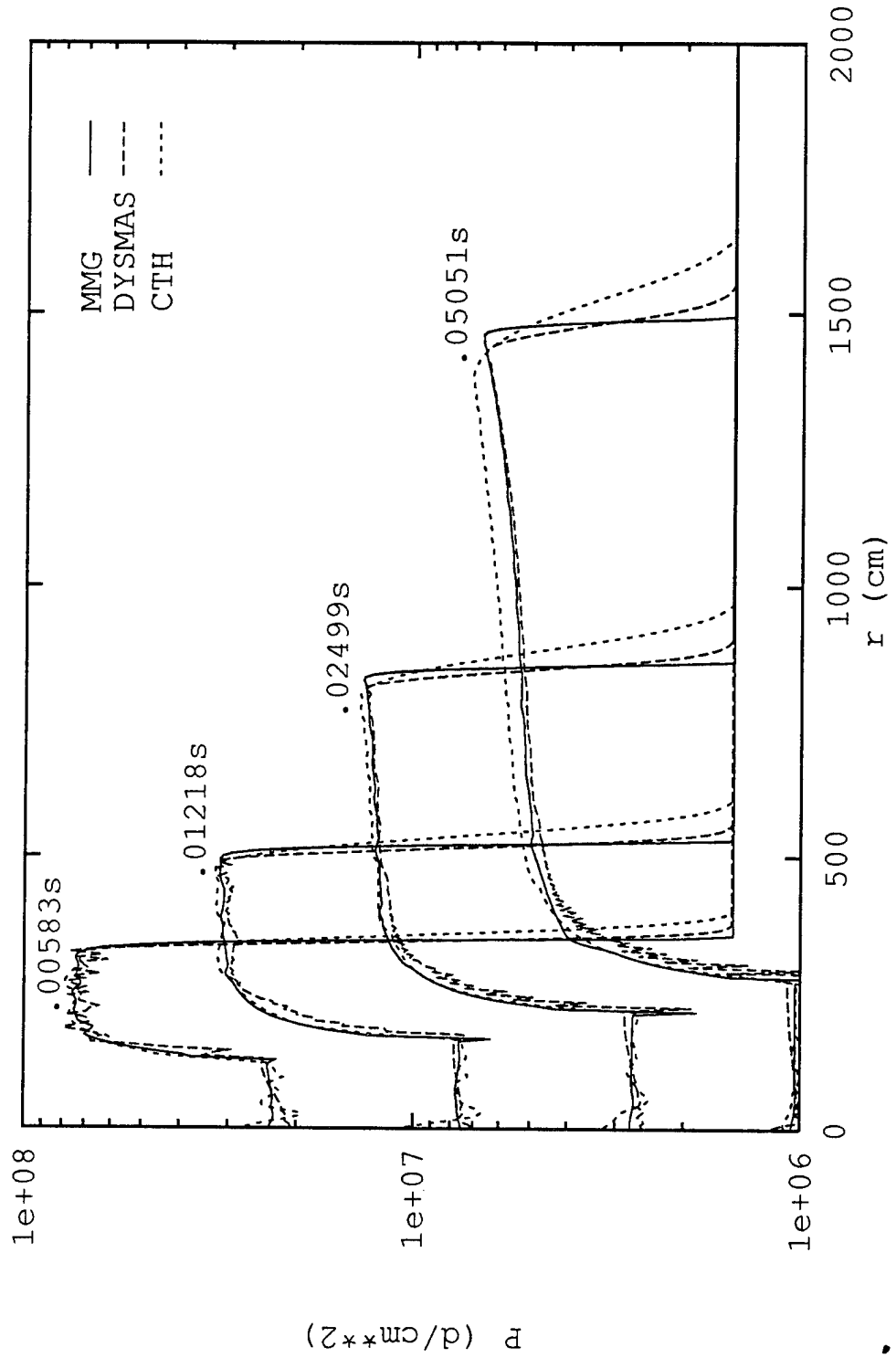

FIGURE 8. PRESSURE RESPONSE OF PARTIALLY SATURATED SAND (α_o=1.052808) TO A GAMMA LAW EXPLOSION BUBBLE

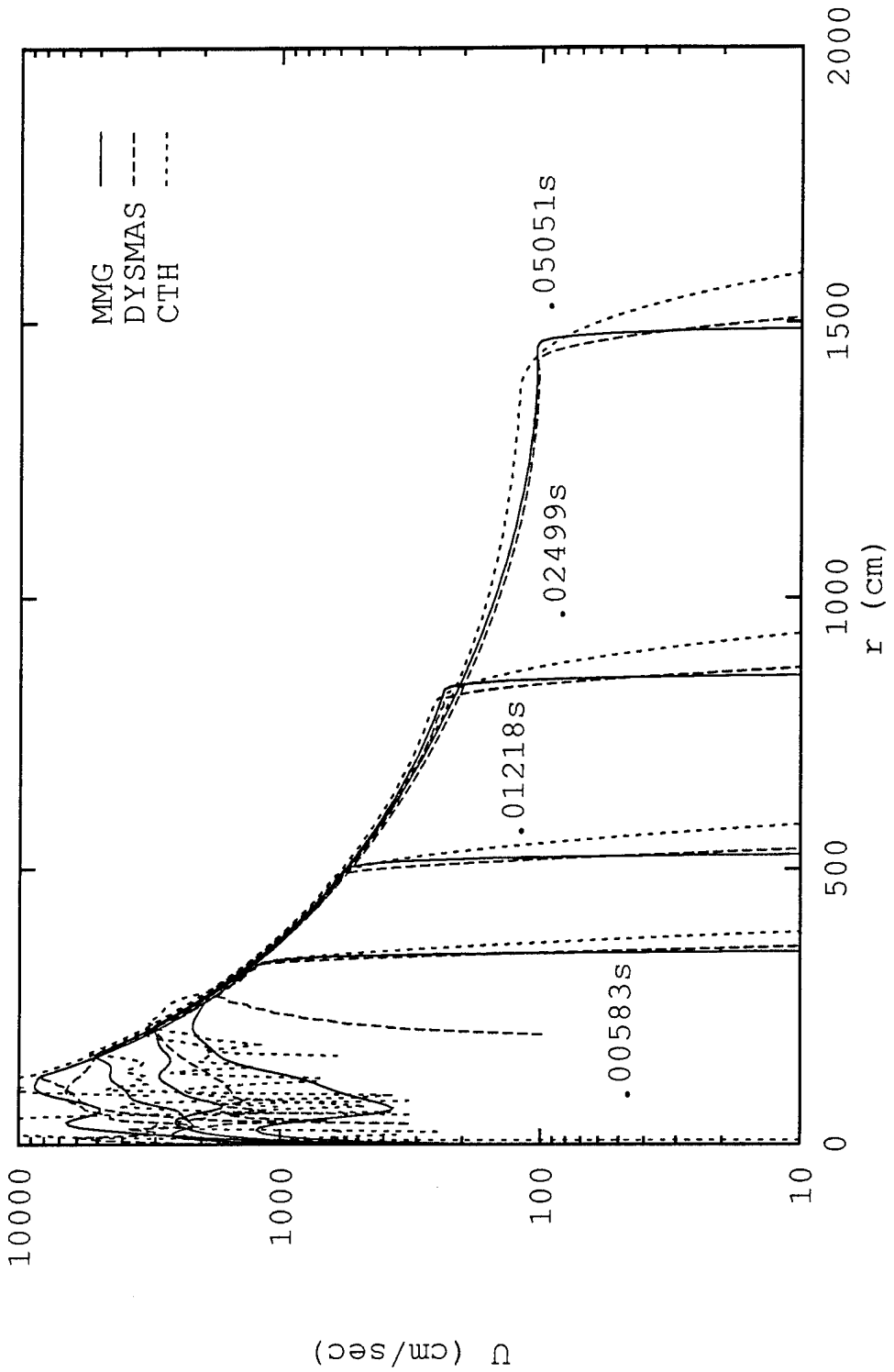

FIGURE 9. VELOCITY RESPONSE OF PARTIALLY SATURATED SAND (α_o=1.052808) TO A GAMMA LAW EXPLOSION BUBBLE

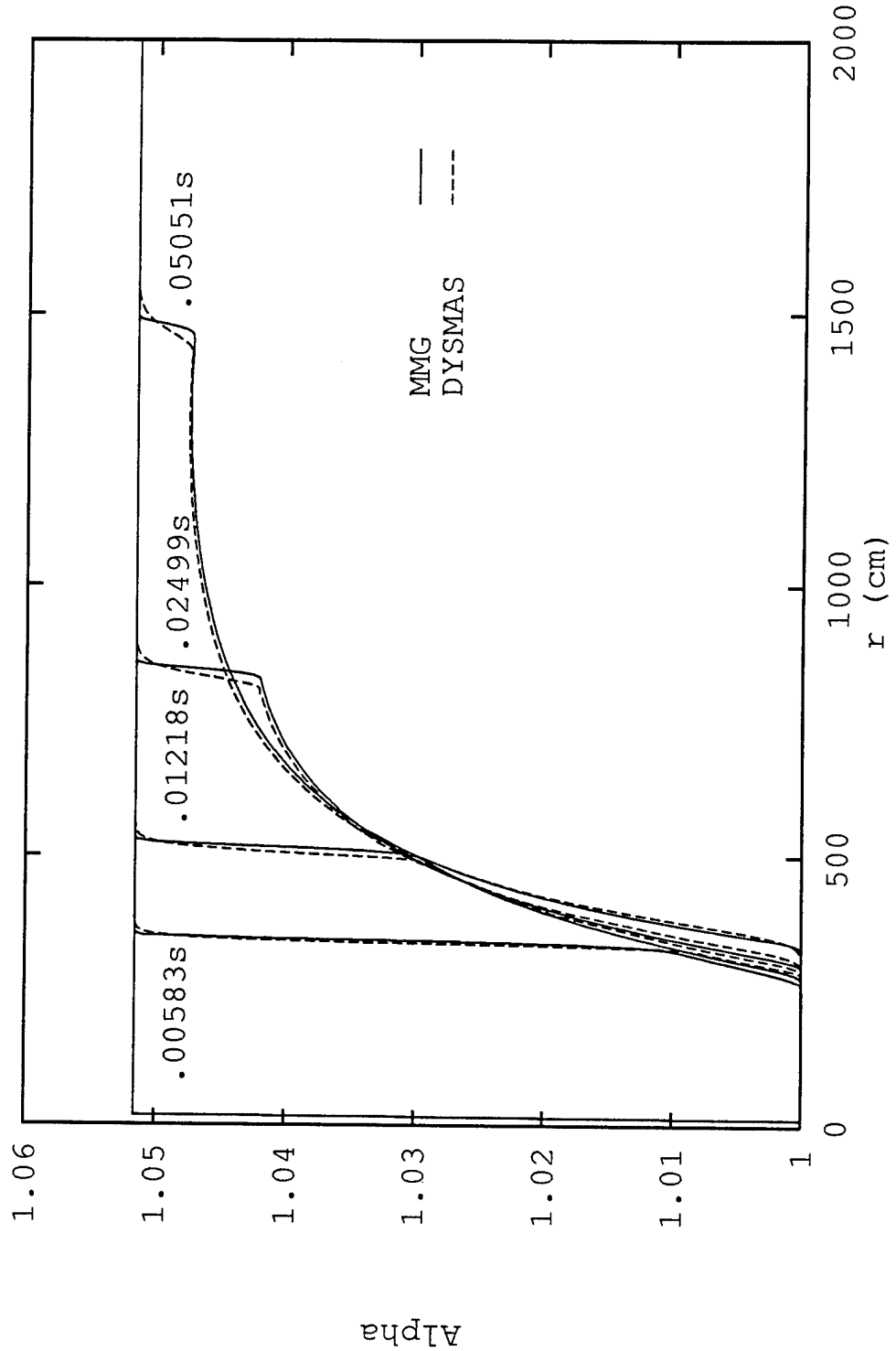

FIGURE 10. COMPUTED α FOR PARTIALLY SATURATED SAND (α_o=1.052808) TO A GAMMA LAW EXPLOSION BUBBLE

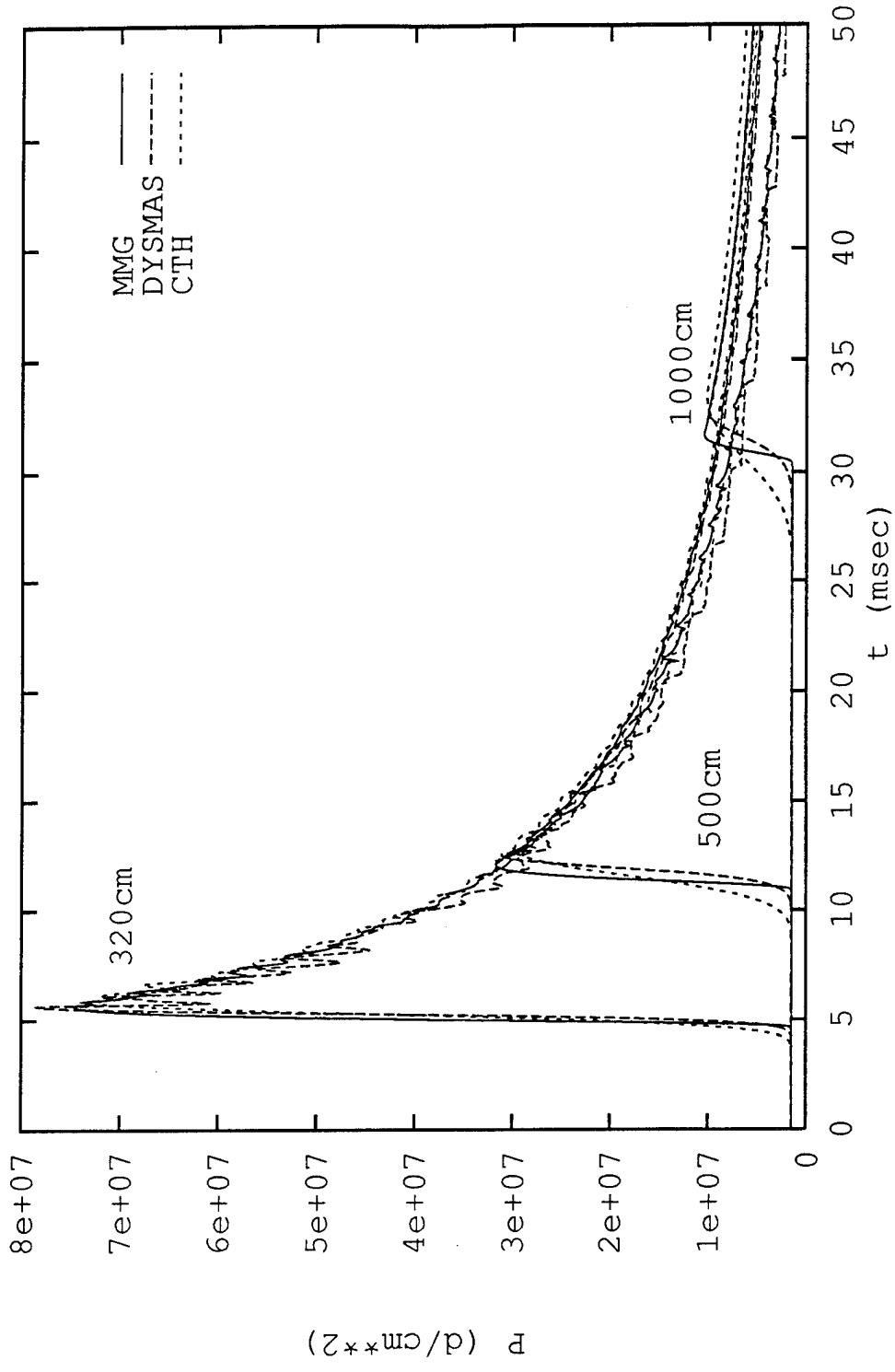

FIGURE 11. PRESSURE HISTORIES AT THREE POINTS FOR PARTIALLY SATURATED SAND (α_o=1.052808) IN RESPONSE TO A GAMMA LAW EXPLOSION BUBBLE

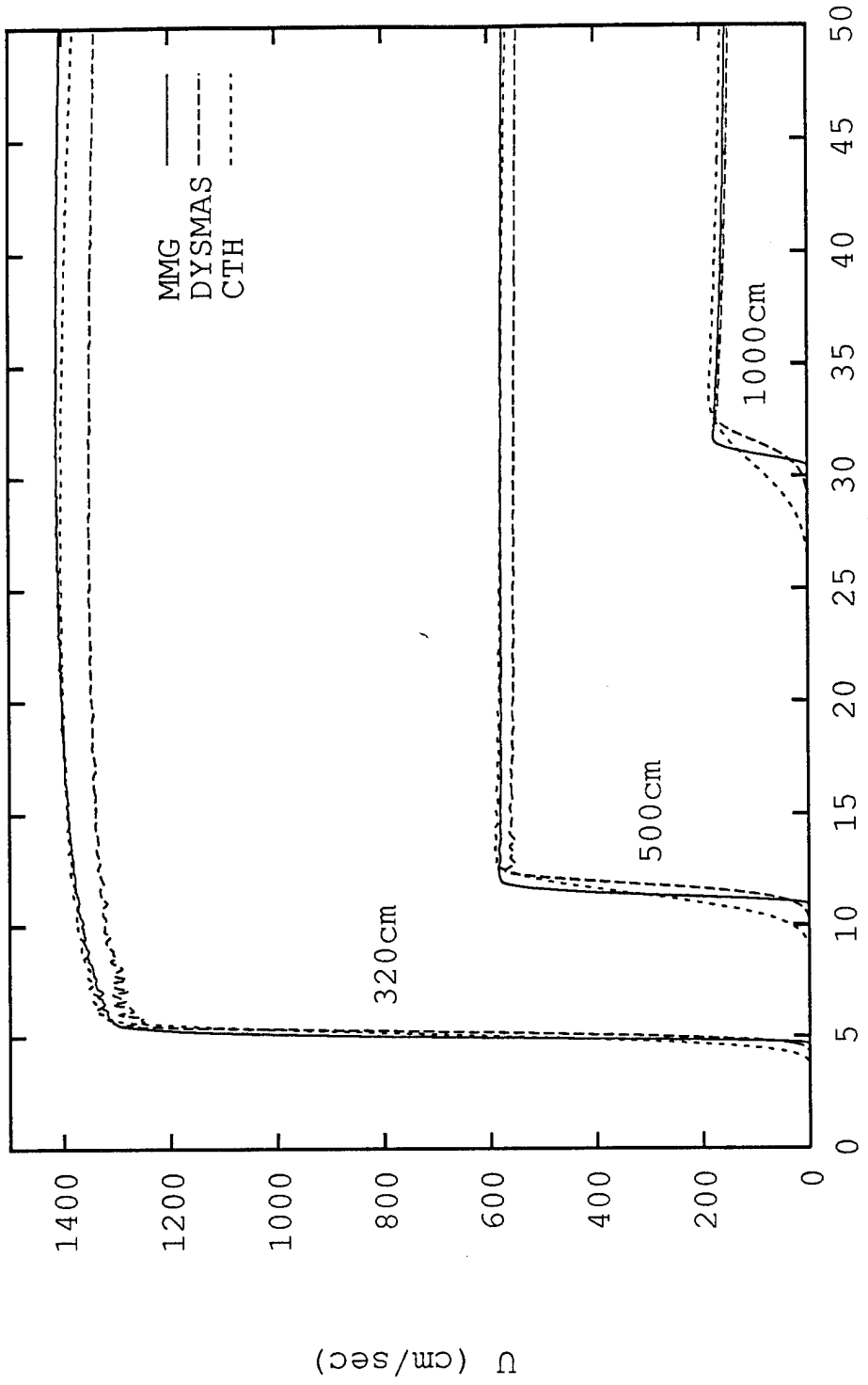

FIGURE 12. VELOCITY HISTORIES AT THREE POINTS FOR PARTIALLY SATURATED SAND (α_o=1.052808) IN RESPONSE TO A GAMMA LAW EXPLOSION BUBBLE

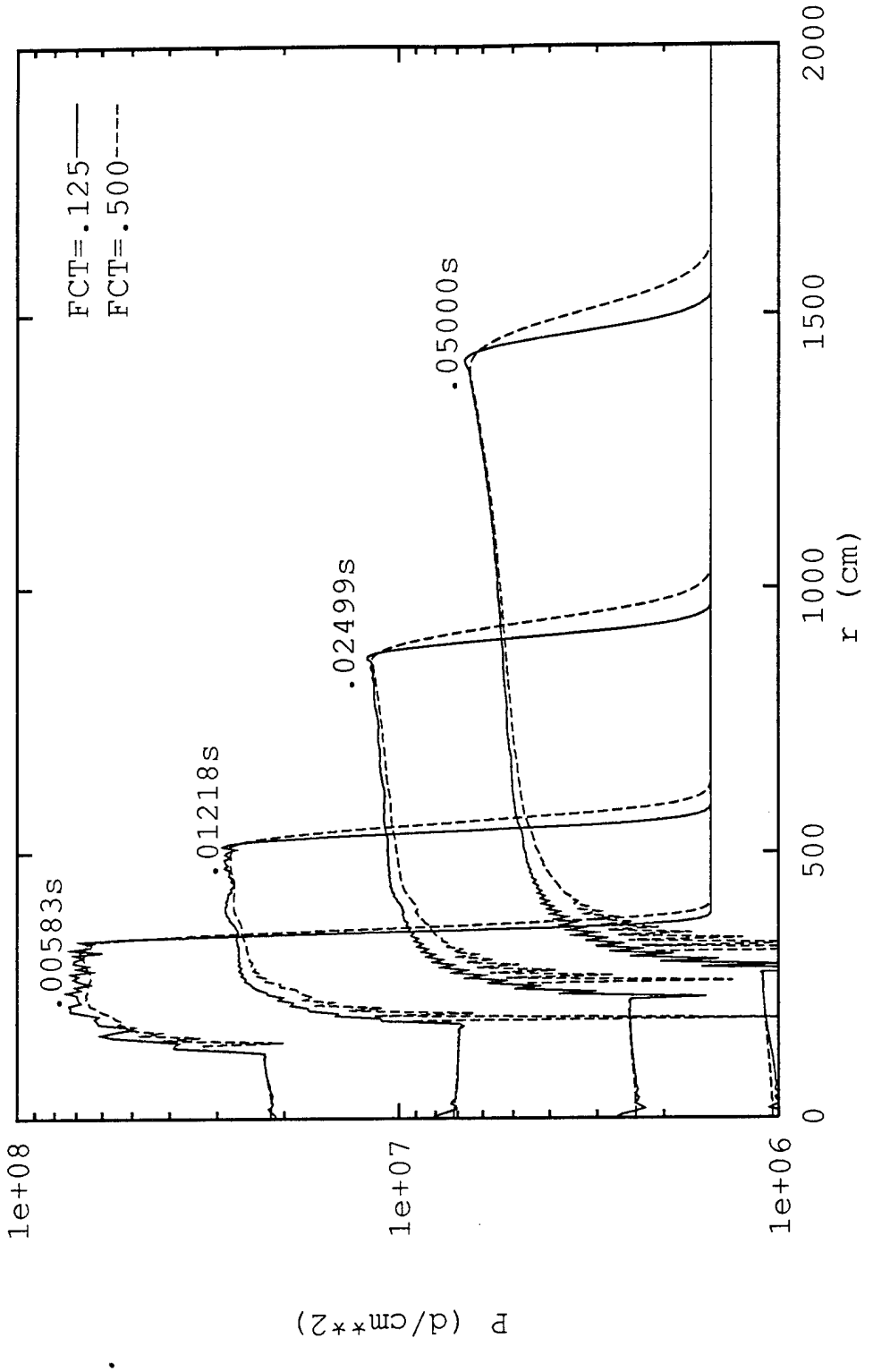

FIGURE 13. INFLUENCE OF FCT PARAMETERS ON THE COMPUTED PRESSURE FOR A GAMMA LAW EXPLOSION BUBBLE.

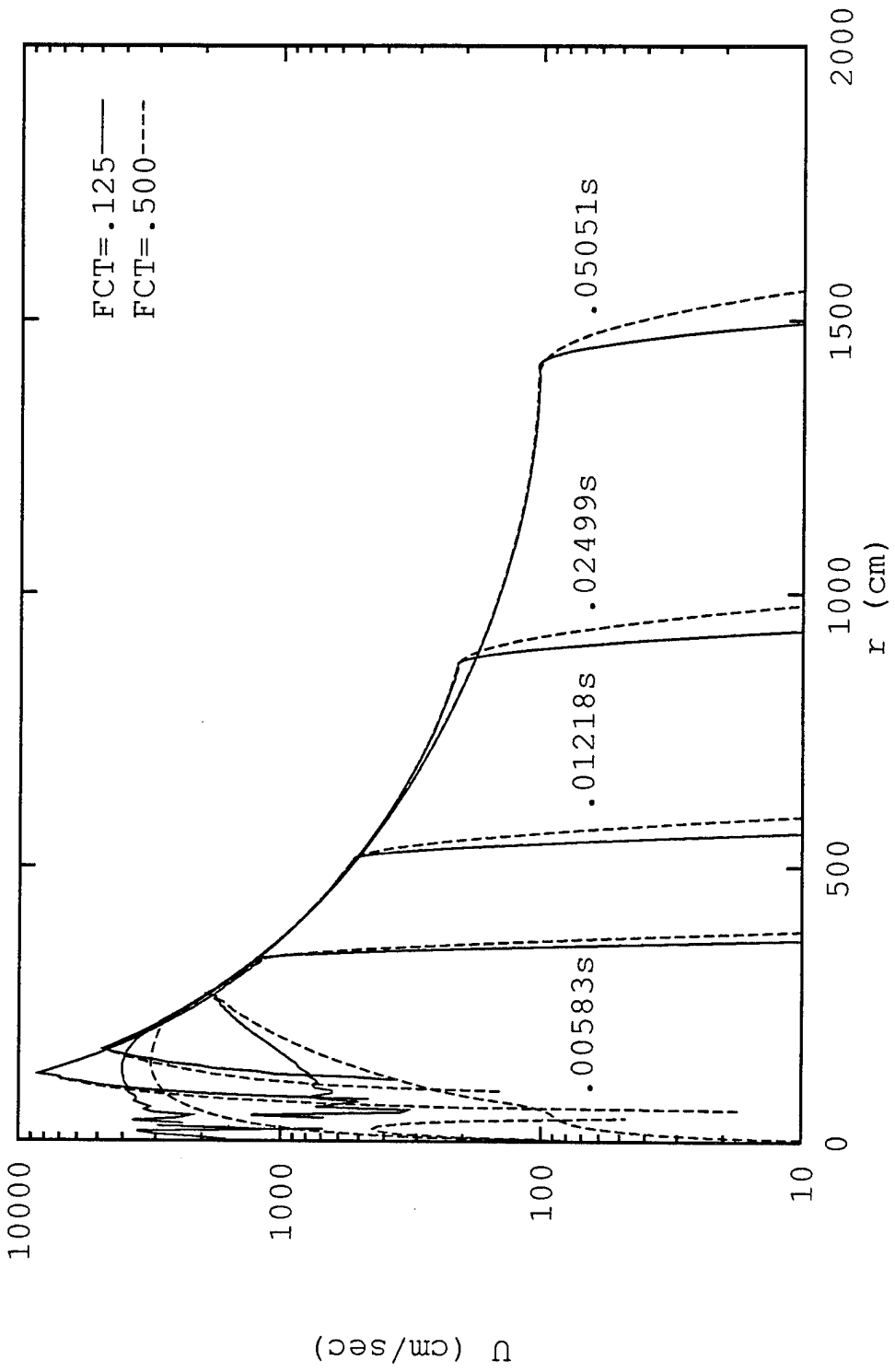

FIGURE 14. INFLUENCE OF FCT PARAMETERS ON THE COMPUTED VELOCITY FOR A GAMMA LAW EXPLOSION BUBBLE.

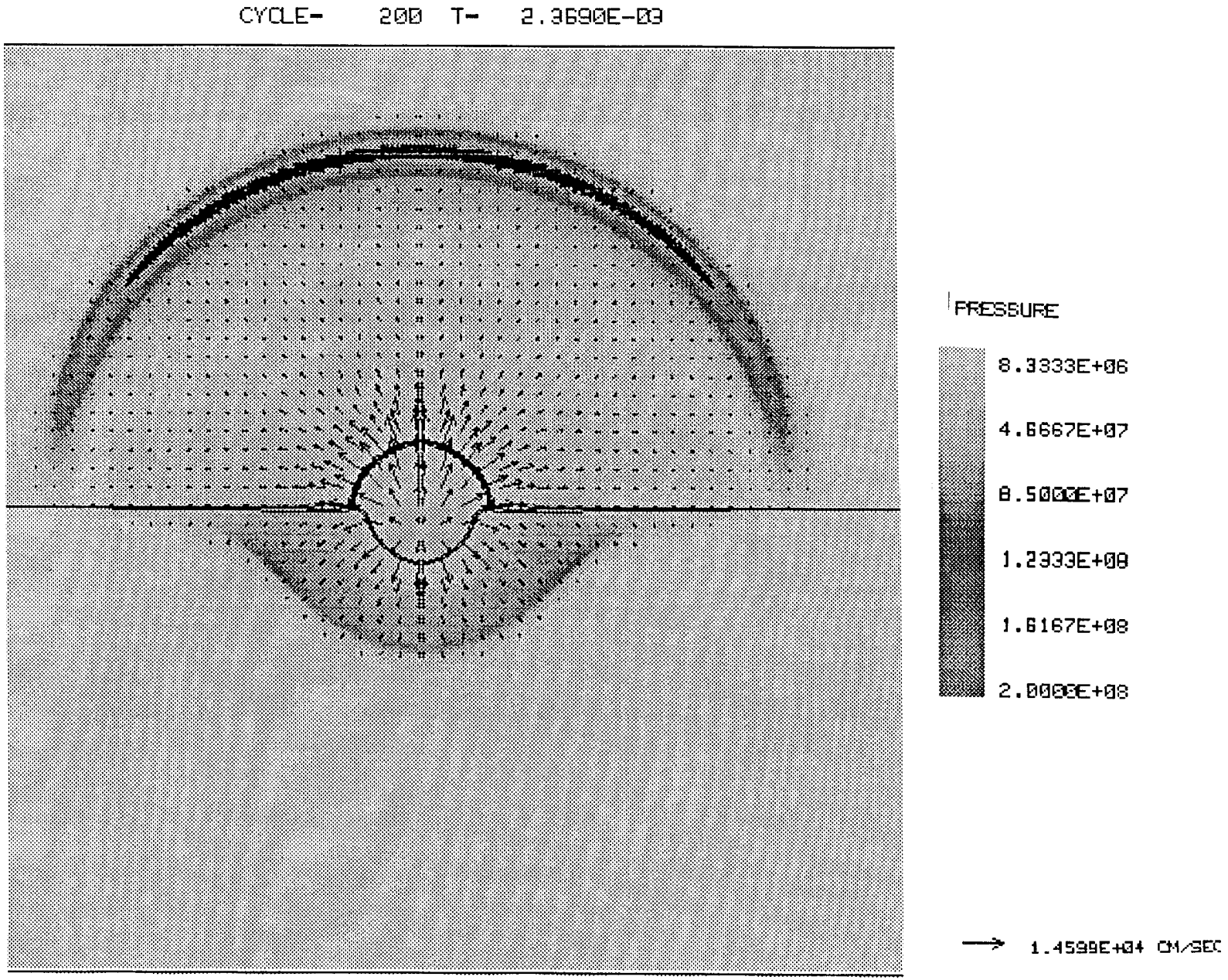

FIGURE 15. GRAY SCALE PRESSURE PLOT FOR AN UNDERWATER TNT EXPLOSION AT THE WATER-SAND INTERFACE.

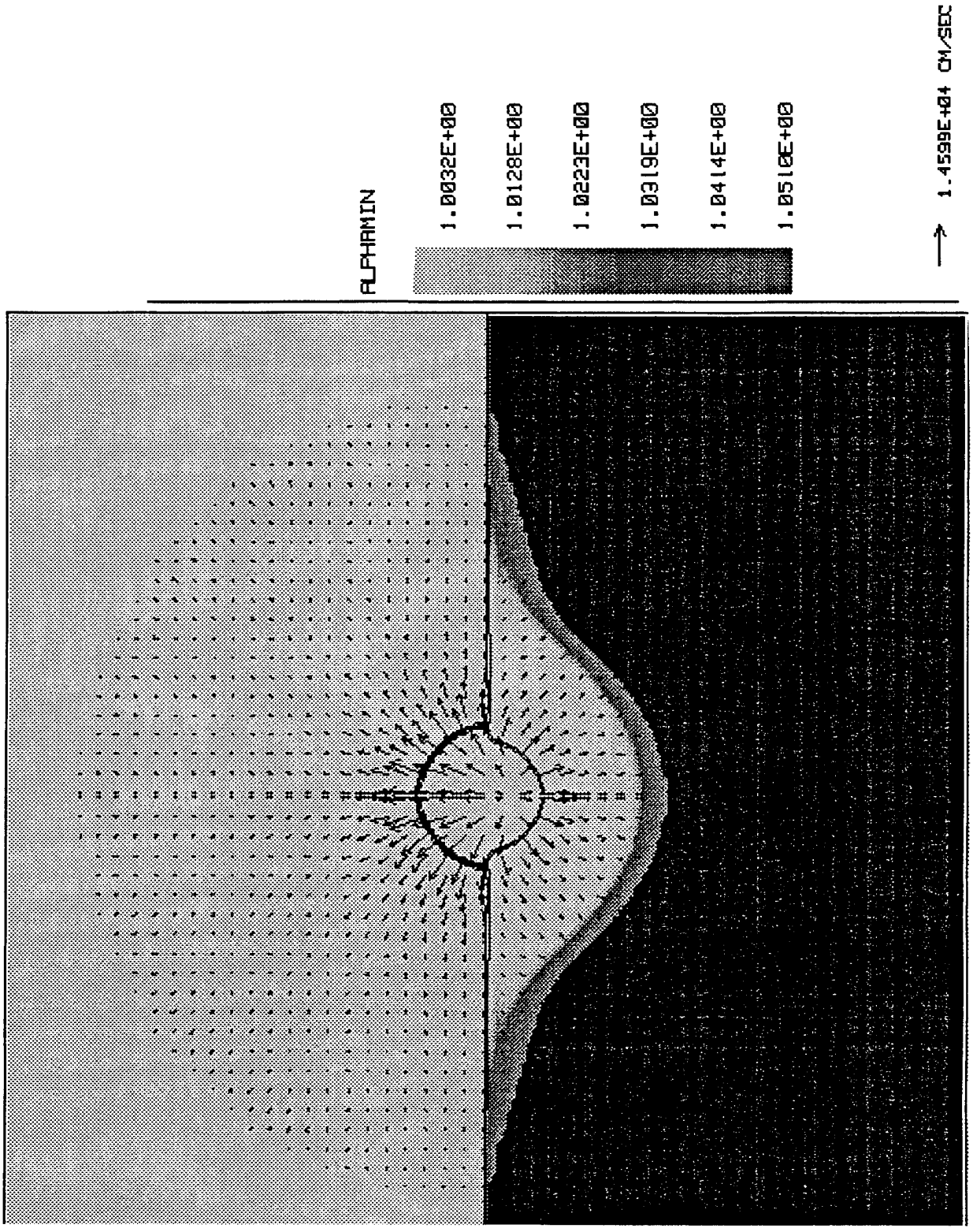

FIGURE 16. GRAY SCALE α PLOT FOR AN UNDERWATER TNT EXPLOSION AT THE WATER-SAND INTERFACE.

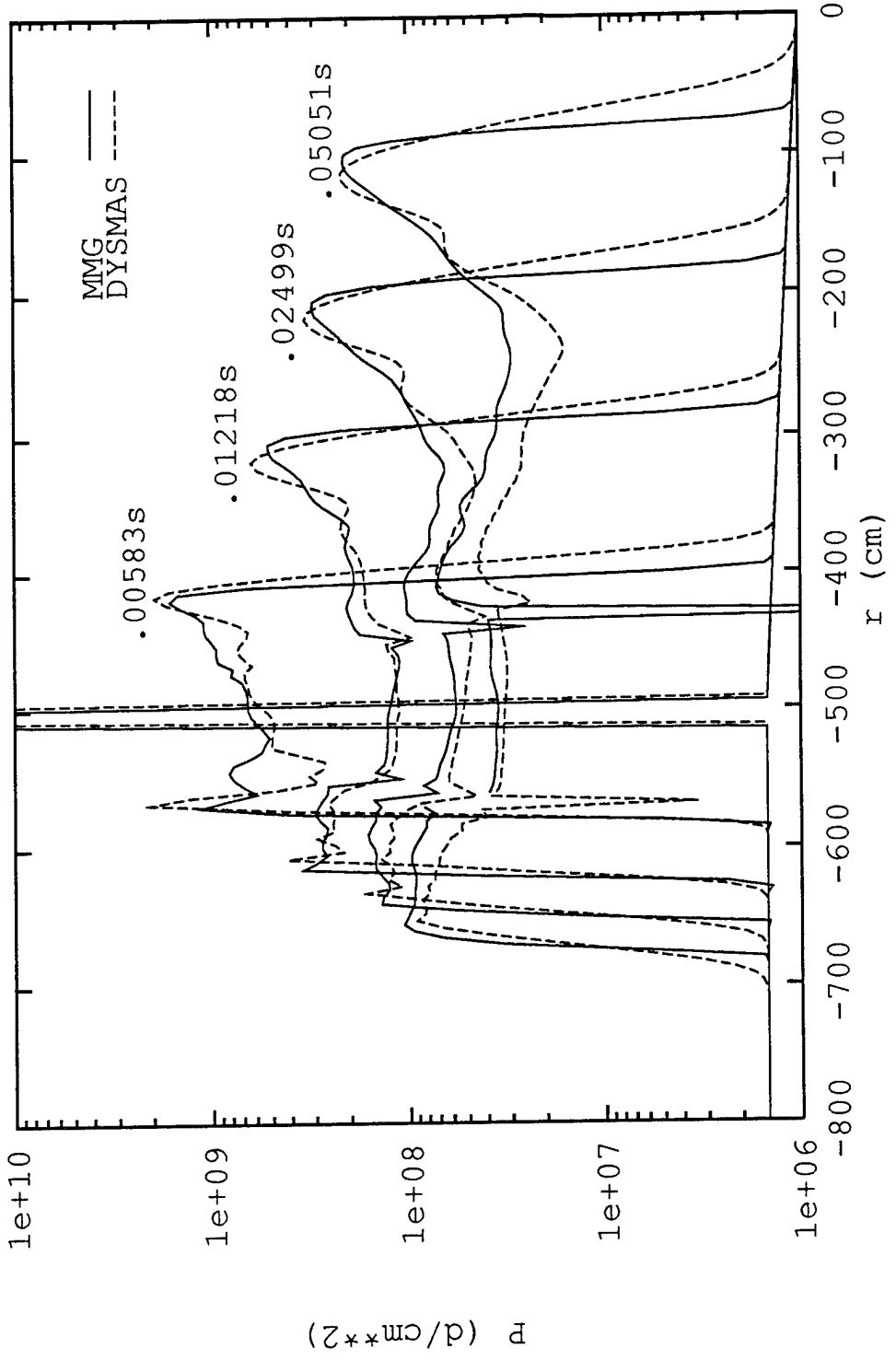

FIGURE 17. PRESSURES ALONG THE CENTERLINE OF THE EXPLOSION OF FIGURES 15 AND 16.

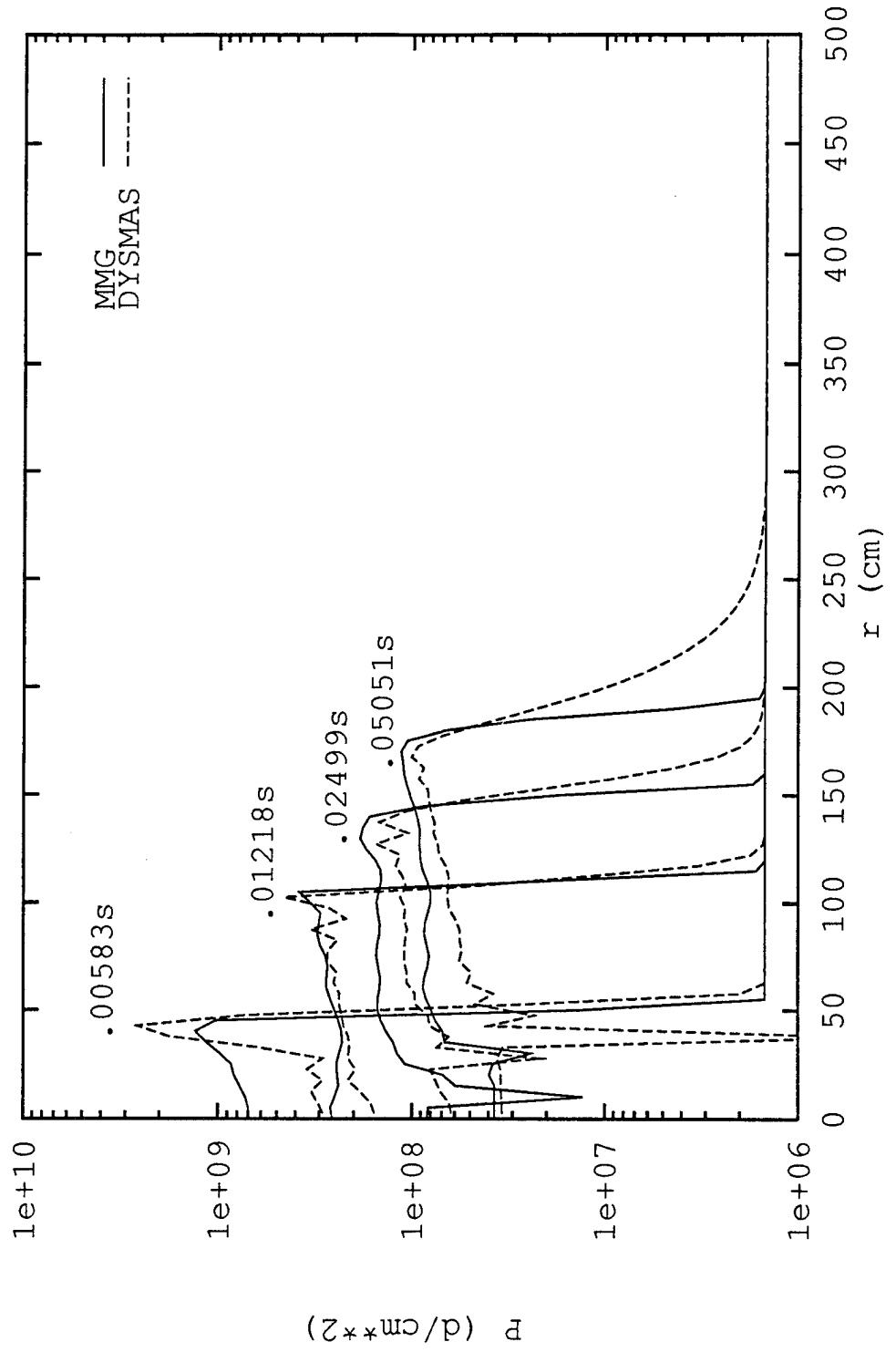

FIGURE 18. PRESSURES ALONG THE z=−550 LINE OF THE EXPLOSION OF FIGURES 15 AND 16.

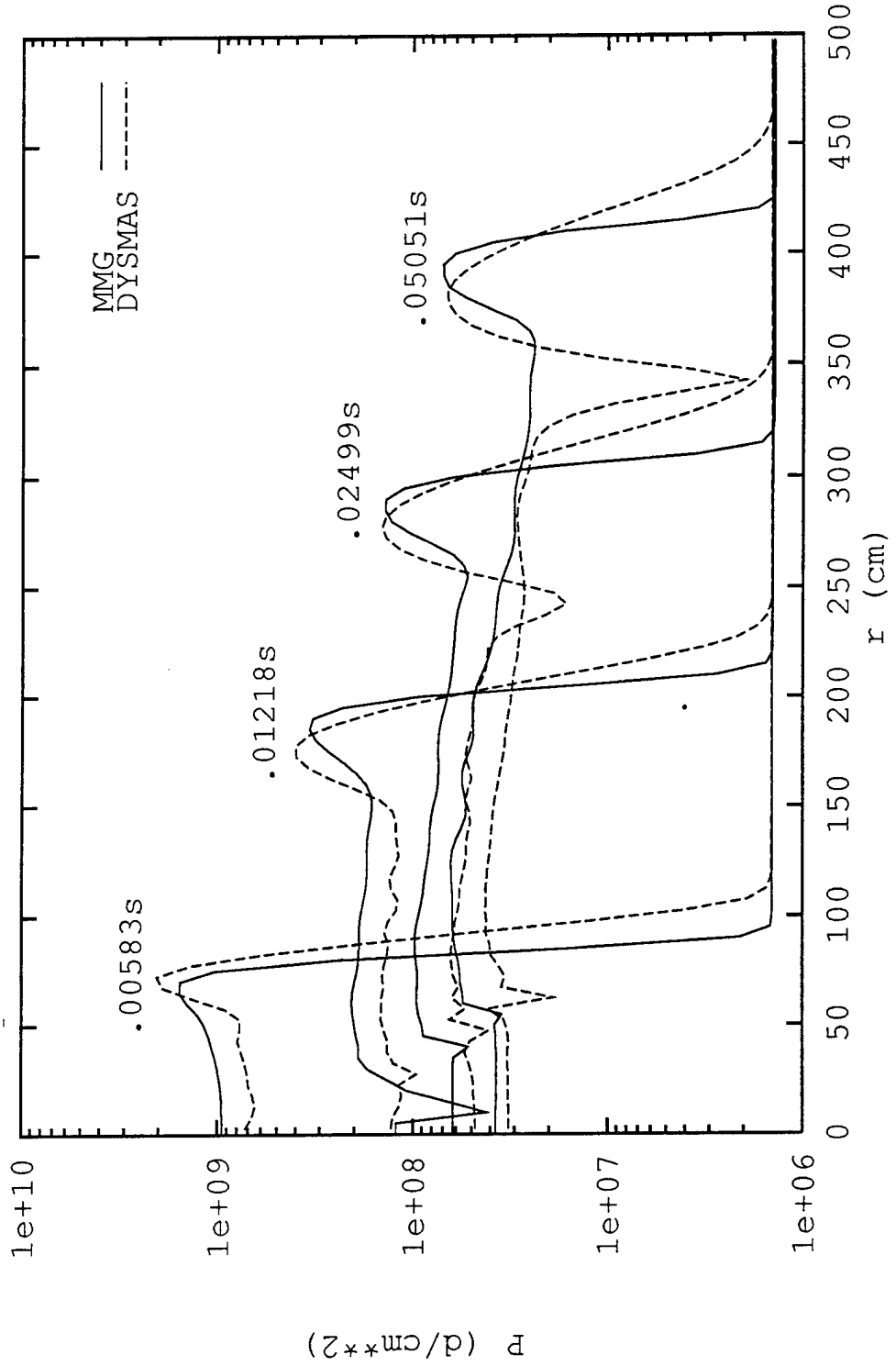

FIGURE 19. PRESSURES ALONG THE z=−450 LINE OF THE EXPLOSION OF FIGURES 15 AND 16.

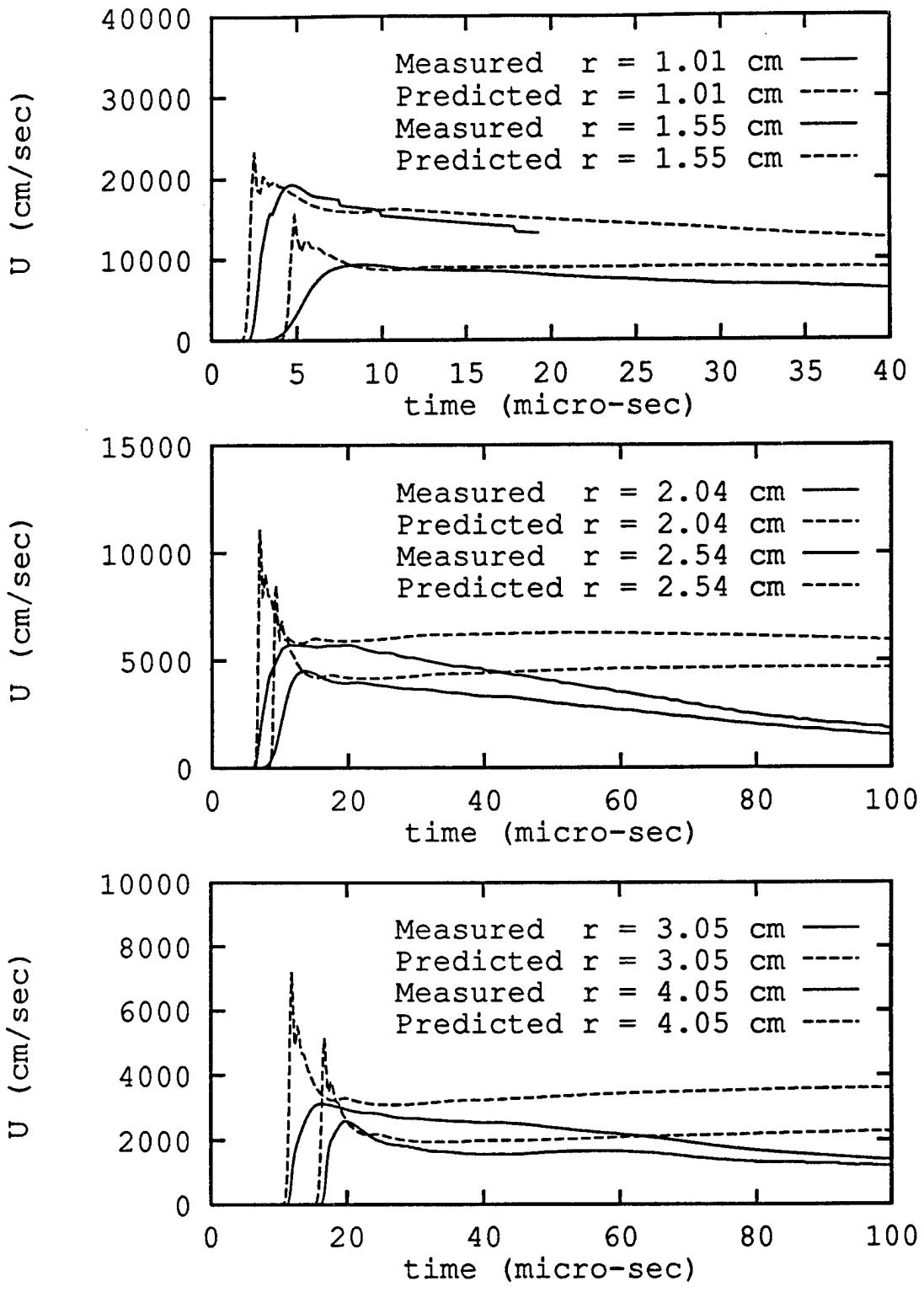

FIGURE 20. COMPUTED AND MEASURED VELOCITIES FOR THE 100% SATURATED SRI TEST.

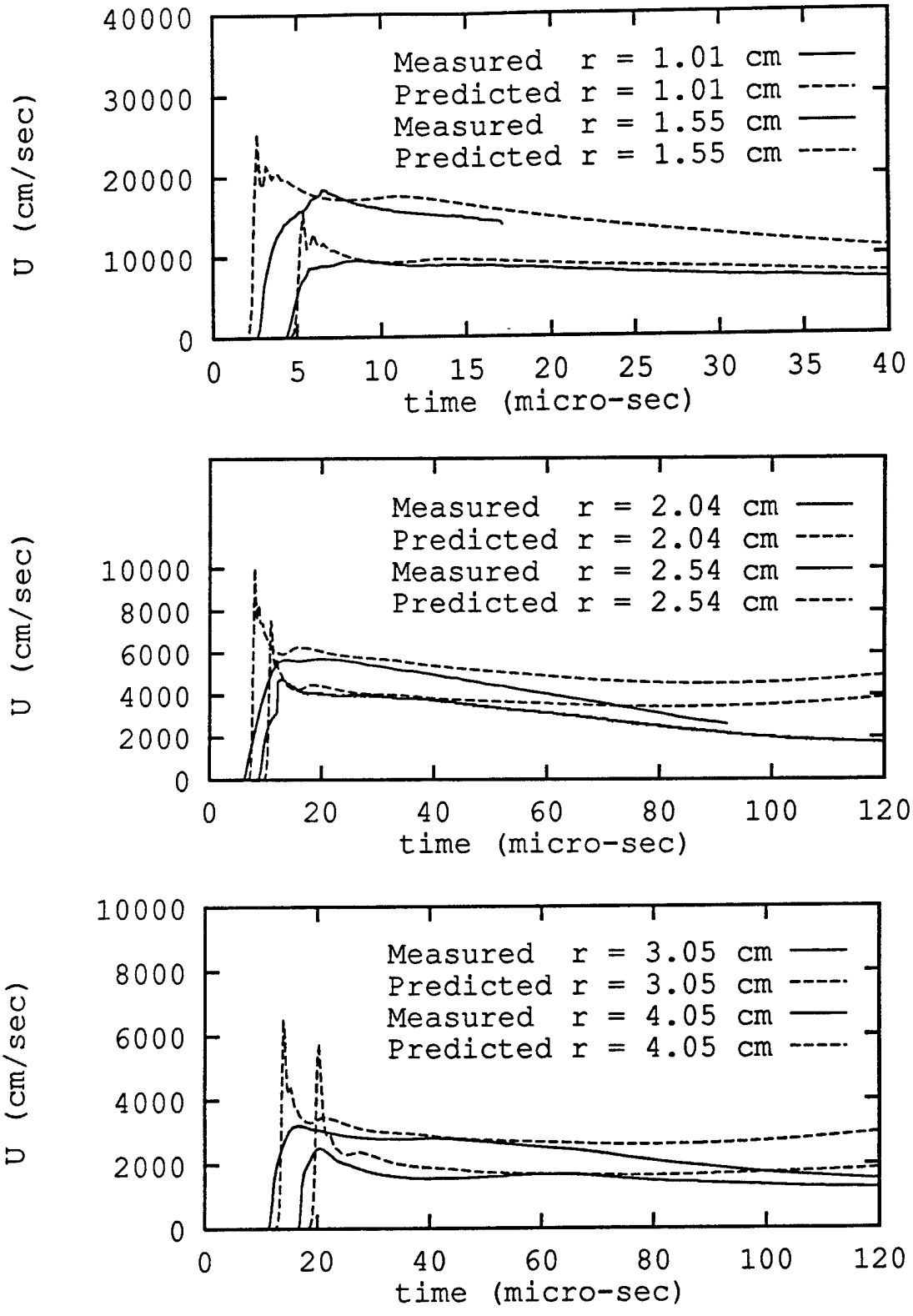

FIGURE 21. . COMPUTED AND MEASURED VELOCITIES FOR THE 95% SATURATED SRI TEST.

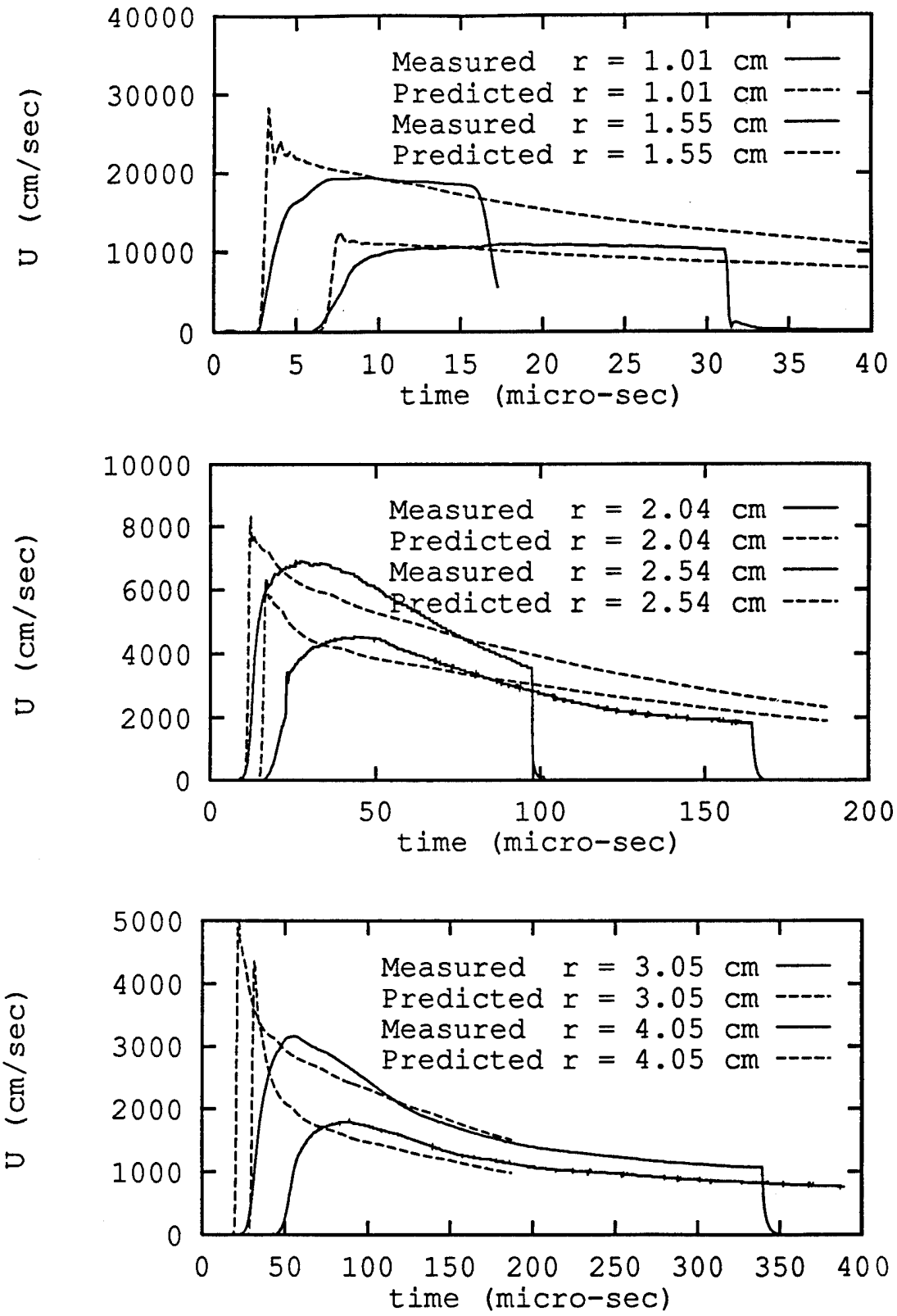

FIGURE 22. COMPUTED AND MEASURED VELOCITIES FOR THE 78% SATURATED SRI TEST.

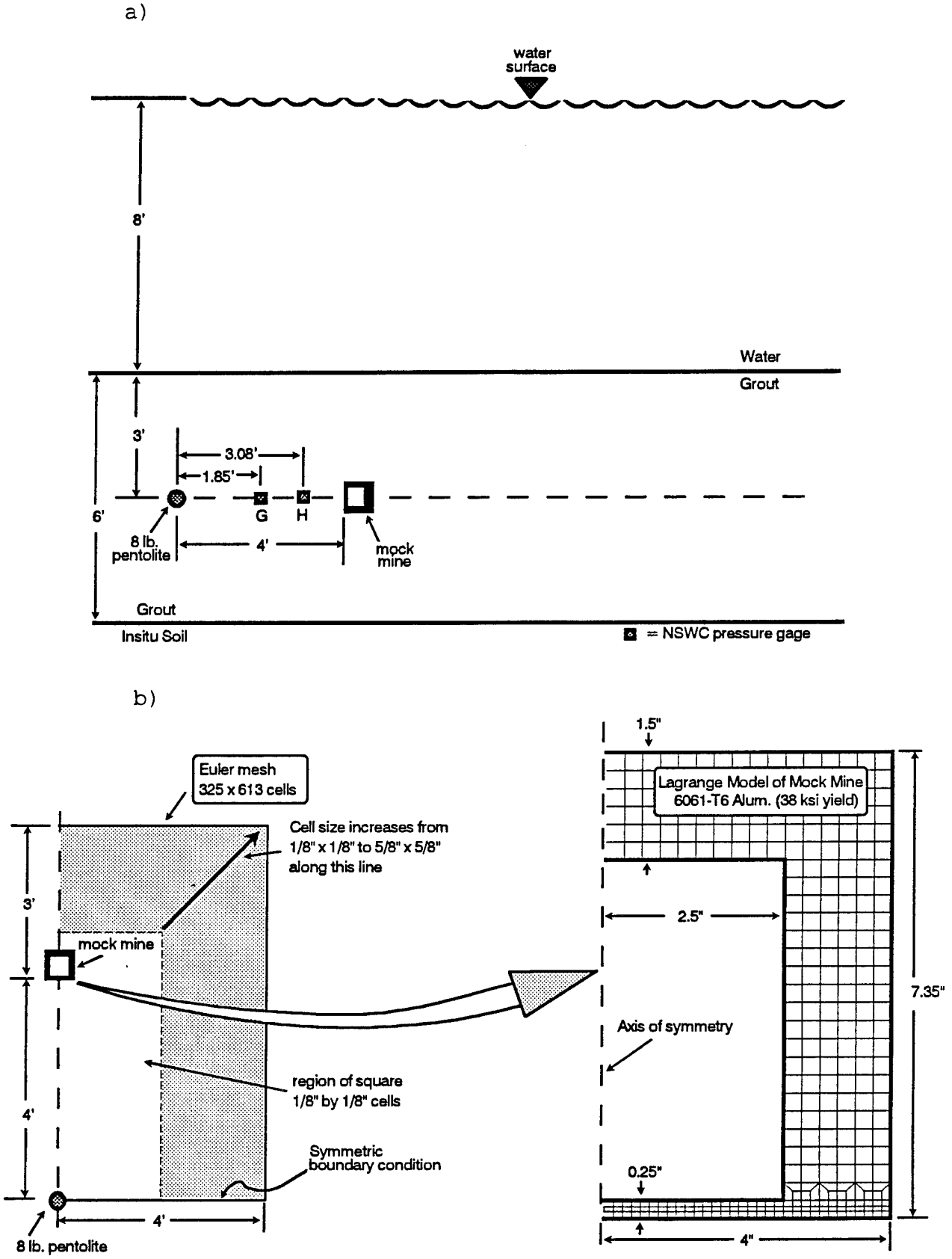

FIGURE 23. SAMSI TEST SETUP

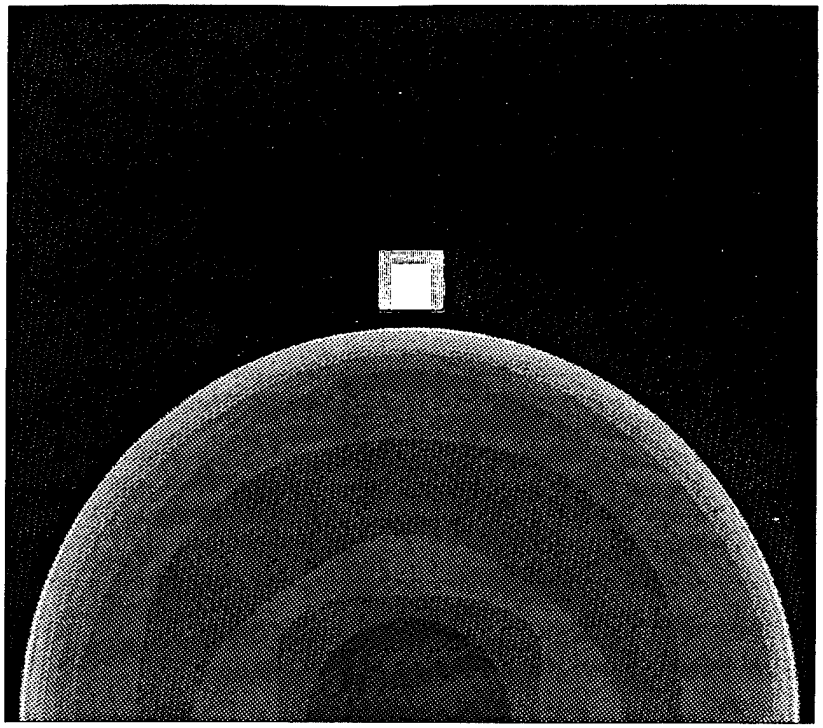

FIGURE 24. COMPUTED PRESSURES FOR THE SAMSI TEST AT 734 μSECS.

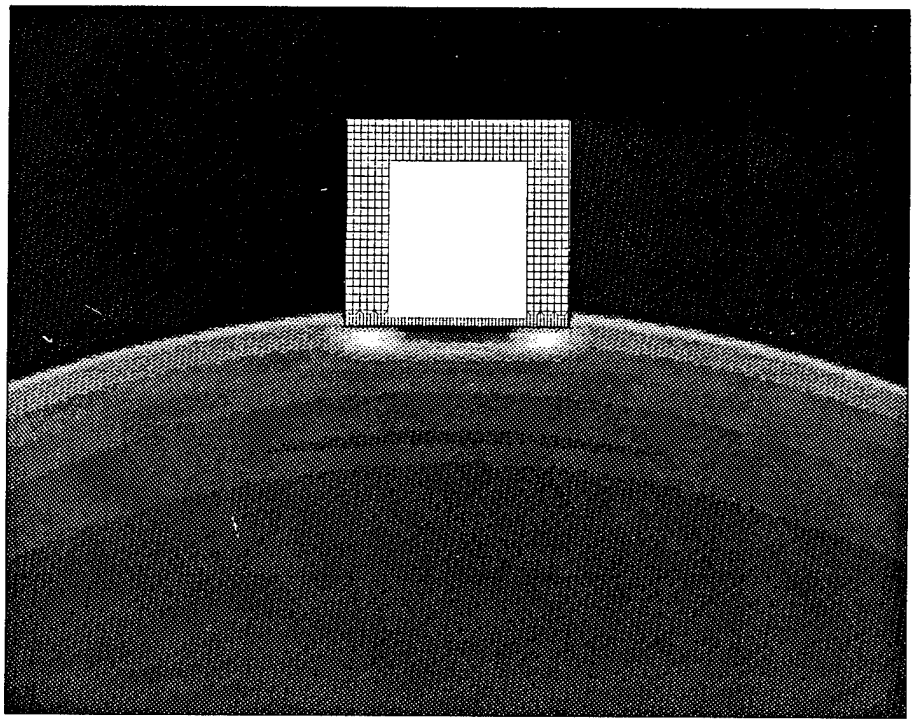

FIGURE 25. COMPUTED PRESSURES FOR THE SAMSI TEST AT 789 μSECS.

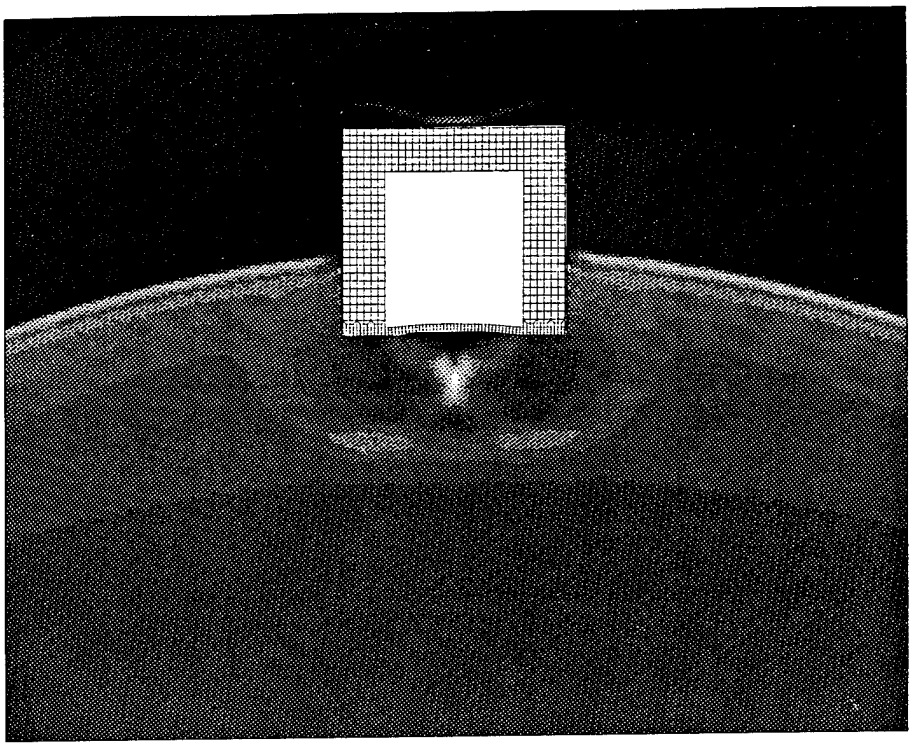

FIGURE 26. COMPUTED PRESSURES FOR THE SAMSI TEST AT 844 μSECS.

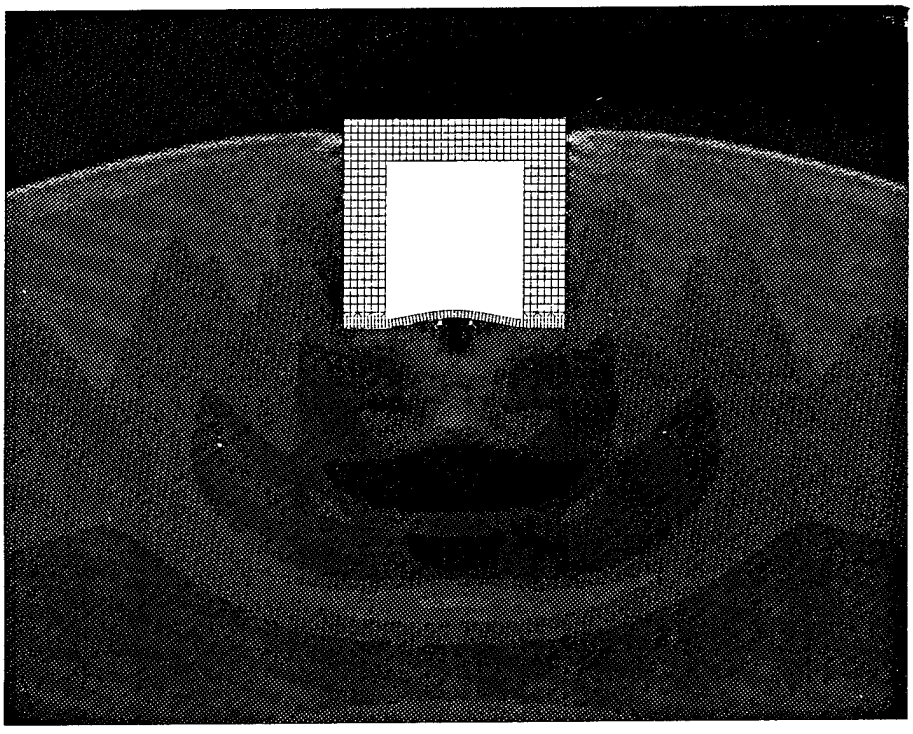

FIGURE 27. COMPUTED PRESSURES FOR THE SAMSI TEST AT 953 μSECS.

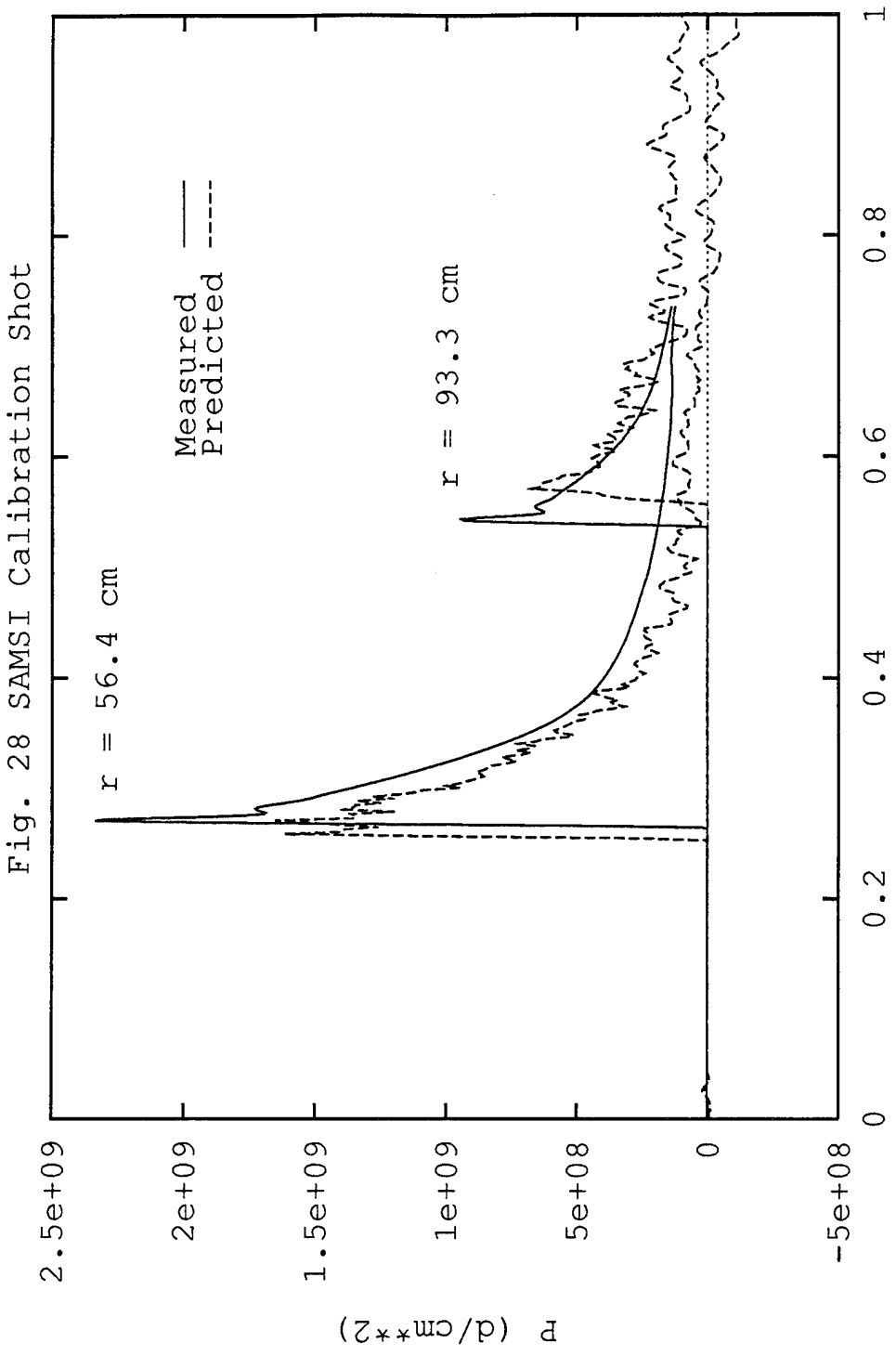

FIGURE 28. COMPUTED AND MEASURED SAND PRESSURES FOR THE SAMSI TEST.

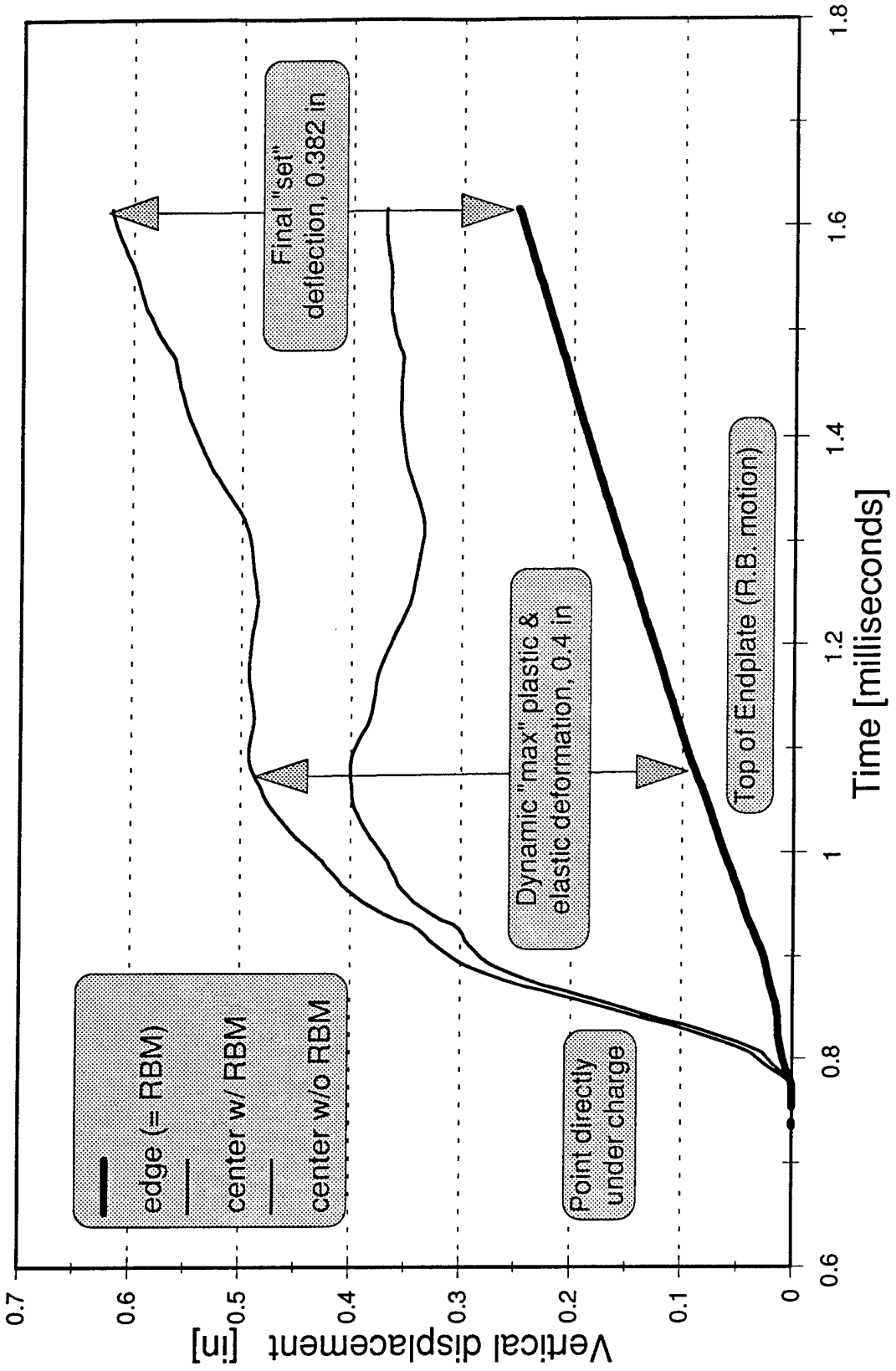

FIGURE 29. COMPUTED CENTERLINE DISPLACEMENT HISTORY FOR THE SAMSI TEST.

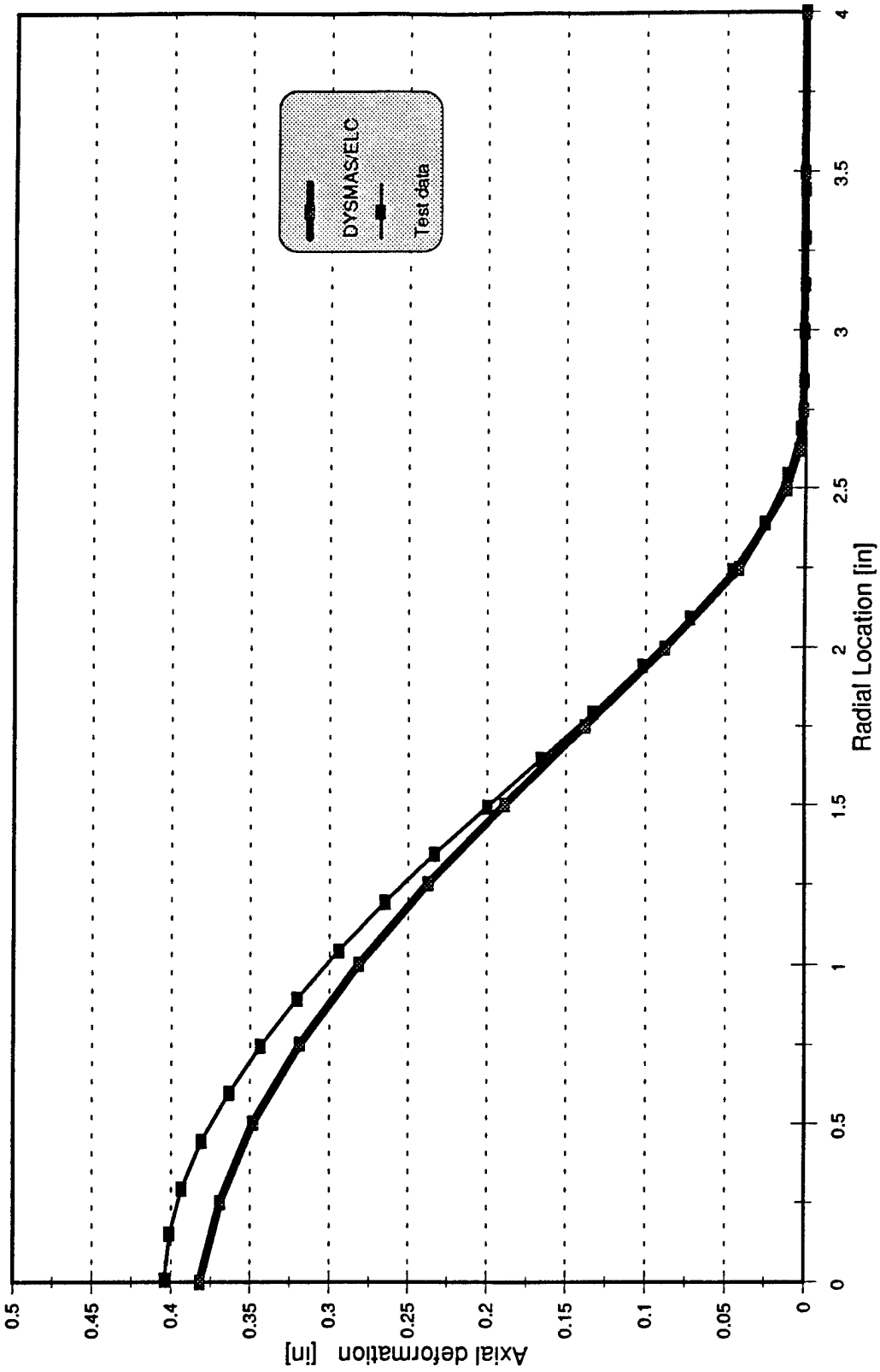

FIGURE 30. COMPUTED AND MEASURED TARGET DEFORMATION FOR THE SAMSI TEST.

APPENDIX A
MIE-GRUENEISEN EQUATION OF STATE ROUTINES

This appendix provides a description of the MieGrueneisen equation of state subroutines.

1. Subroutine STDMIE: $f_1(\Delta\rho_1, \Delta e_1) \rightarrow (\Delta p_1, c_1^2, \Delta p_{r_1}, \Delta e_{r_1})$

   a. Function: Compute $\Delta p_1, c_1^2$ given $\Delta\rho_1, \Delta e_1$.
   b. Description: Evaluate appropriate equations.
   c. Algorithm: Solve Eq. (22) for Δp and Eq. (23) for c^2. Evaluating these equations requires use of Eqs. (2)-(6), (11) and also produces $\Delta p_{r_1}, \Delta e_{r_1}$.

2. Subroutine ISEMIE: $f_2(\Delta\rho_1, \Delta e_1, \Delta\rho_2) \rightarrow (\Delta p_2, \Delta e_2, c_2^2)$

   a. Function: Compute $\Delta p_2, \Delta e_2, c_2^2$ given $\Delta\rho_1, \Delta e_1, \rho_2$ and assuming an isentropic change of state between $\Delta\rho_1$ *and* $\Delta\rho_2$.
   b. Description: Evaluate Equation (25)
   c. Algorithm:

      $f_1(\Delta\rho_1, \Delta e_1) \rightarrow (\Delta p_1, c_1^2, \Delta p_{r_1}, \Delta e_{r_1})$
      $f_1(\Delta\rho_2, \Delta e_1) \rightarrow (\Delta p_t, c_t, \Delta p_{r_2}, \Delta e_{r_2})$
      compute Δe_2 from Eq. (16) and solve Equation (22) for Δp_2.
      Re-evaluate c: $c^2 = c_t^2 + \Gamma_o \rho_o (\Delta p_2 - \Delta p_t)/\rho_2^2$

3. Subroutine HUGMIE: $f_3(\Delta\rho_1, \Delta e_1, \Delta\rho_2) \rightarrow (\Delta p_2, \Delta e_2, c_2^2)$

   a. Function: Compute $\Delta p_2, \Delta e_2, c_2^2$ given $\Delta\rho_1, \Delta e_1, \Delta\rho_2$ and assuming a change of state along the Hugoniot $\Delta\rho_1$ *and* $\Delta\rho_2$.
   b. Description: Evaluate Equation (26).
   c. Algorithm:

      $f_1(\Delta\rho_1, \Delta e_1) \rightarrow (\Delta p_1, c_1^2, \Delta p_{r_1}, \Delta e_{r_1})$
      $f_1(\Delta\rho_2, \Delta e_1) \rightarrow (\Delta p_t, c_t, \Delta p_{r_2}, \Delta e_{r_2})$
      Compute δp from Eq. (26).
      $\Delta p_2 = \Delta p_1 + \delta p$
      Solve Eq. (22) for Δe_2.
      Re-evaluate c: $c^2 = c_t^2 + \Gamma_o \rho_o (\Delta p_2 - \Delta p_t)/\rho_2^2$

4. Subroutine ISTMIE: $f_4(\Delta p_1, \Delta e_1) \rightarrow (\Delta\rho_1, c_1^2)$

   a. Function: Compute $\Delta\rho_1, c_1^2$ given $\Delta p_1, \Delta e_1$
   b. Description: Iterate for the value of ρ which statisfies Equation (22).
   c. Algorithm:

      $\Delta\rho^0 = 0$
      Iterate from n=1 until convergence or n > maximum number of iteration.

      $f_1(\Delta\rho_1^{n-1}, \Delta e) \rightarrow (\Delta p^n, c^{2^n})$
      compute $\left(\frac{\partial\Delta p}{\partial\Delta\rho}\right)_e$ from Eq. (12).
      Compute $\delta\rho^n = (\Delta p_2 - \Delta p^n)/\left(\frac{\partial\Delta p}{\partial\Delta\rho}\right)_e$

if $\delta\rho^n < 10^{-6}$ iteration is complete. Otherwise:

$$\Delta\rho^n = \Delta\rho^{n-1} + min[max(\delta\rho^n, -.2), .2] \tag{1}$$

Set: $\Delta\rho_1 = \Delta\rho^n; \quad c = c^n$

5. Subroutine IISMIE: $f_5(\Delta p_1, \Delta e_1, \Delta p_2) \rightarrow (\Delta\rho_2, \Delta e_2, c_2^2)$
   a. Function: Compute ρ_2, e_2, c_2^2 given p_1, e_1, p_2 and assuming an isentropic change of state from Δp_1 *and* Δp_2.
   b. Description: Apply ISTMIE to determine initial density. Iterate for a final value of rho which is on the same isentrop as the initial conditions and has a pressure value equal to p_2
   c. Algorithm:

$f_4(\Delta\rho_1, \Delta e_1) \rightarrow (\Delta p_1, c_1^{2^n})$
$\delta\rho^0 = (\Delta p_2 - \Delta p_1)/c^2; \ \Delta e_2^0 = \Delta e_1; \Delta\rho^0 = \Delta\rho_1$
Iterate from n=1 until convergence or n > maximum number of iteration.

$\Delta\rho^n = \Delta\rho^{n-1} + min[max(\delta\rho^n, -.2), .2]$
$f_1(\Delta\rho^n, \Delta e^{n-1}) \rightarrow (\Delta p_t, \Delta e_{r_2}, c_t^2)$
Solve Eq. (25) for Δe^n
Solve Eq. (22) for Δp^n
Re-evaluate c_t: $c_{t_1}^2 = c_t^2 + \Gamma_o\rho_o(\Delta p^n - \Delta p_t)/\rho_2^2$
$\delta\rho^n = (\Delta p^2 - \Delta p^n)/c_{t_1}^2$
If $\delta\rho^n < 10^{-6}$ iteration is complete.

$\Delta\rho_2 = \Delta\rho^n; \quad \Delta e_2 = \Delta e^n$

6. Subroutine IHUMIE: $f_6(\Delta p_1, \Delta e_1, \Delta p_2) \rightarrow (\Delta\rho_2, \Delta e_2, c_2^2)$
   a. Function: Compute ρ_2, e_2, c_2^2 given p_1, e_1, p_2 and assuming a change of state along the Hugoniot from Δp_1 *and* Δp_2.
   b. Description: Apple ISTMIE to determine the initial density. Iteratre for a final value of denity which as along Hugoniot and produces the pressure p_2
   c. Algorithm:

$f_3(\Delta p_1, \Delta e_1) \rightarrow (\Delta\rho_1, c_2^2)$
Iterate from n = 1 until convergence or n > maximum number of iterations. Start iteration with: $\delta\rho^1 = \delta p/c_1^2; \ \Delta e^0 = \Delta e_1; \ \Delta\rho^0 = \Delta\rho_1$

$\Delta\rho^n = \Delta\rho^{n-1} + min[max(\delta\rho^n, -.2), .2]$
Solve Eq. (17) for Δe^2 and set $\Delta e^n = \Delta e^2$
$f_1(\Delta\rho_1, \Delta e_1) \rightarrow (\Delta p^n, \Delta e_{r_2} c_t^2)$
$\delta\rho^{'} = (\Delta p_2 - \Delta p^n)/c_t^2$

If $\delta\rho' < 10^{-6}$, iteration is complete. Otherwise :

$$\delta\rho^n = -\delta\rho' \Big/ \left(\frac{\delta\rho' - \delta\rho^{n-1}}{\Delta\rho^n - \Delta\rho^{n-1}} \right) \quad if\ n > 1$$
$$\delta\rho^n = -\delta\rho' \qquad\qquad n = 1 \tag{2}$$

$$\Delta\rho_2 = \Delta\rho_1 + \delta\rho' \ ; \qquad \Delta e_2 = \Delta e^n$$

APPENDIX B
P-α EQUATION OF STATE ROUTINES

This appendix provides a description of the P-α equation of state subroutines. In many cases the Mie-Grueneisen Equation of State are called

1. Subroutine STDP_A: $F_1(\Delta\rho_1, \Delta e_1, \alpha_{min}) \rightarrow (\Delta p_1, c_1^2, \Delta p_{r_1}, \Delta e_{r_1}, \alpha_1)$

   a. Function: Compute $\Delta p_1, c_1^2, \alpha_1$ given $\Delta\rho_1, \Delta e_1, \alpha_{min}$.
   b. Description: Solves Equation (39) Iteratively
   c. Algorithm:

      Check for the solid case. If $p(1, \rho, e) \geq p_s$ *or* $\alpha_{min} = 1$ then material is compressed to a solid and $p = p(1, \rho, e)$ *and* $\alpha = 1$
      Otherwise, check plastic case. If $p(\alpha_{min}, \rho, e) > P_{pl}(\alpha_{min}, \alpha_{min})$, use Newton iteration to solve$p(\alpha, \rho, e) = P_{pl}(p, \alpha_{min})$.
      Else the case is elastic. Apply a Newton iteration to solve $p(\alpha, \rho, e) = P_{el}(p, \alpha_{min})$.

2. Subroutine ISEP_A: $F_2(\Delta\rho_1, \Delta e_1, \Delta\rho_2, \alpha_{min}) \rightarrow (\Delta p_2, \Delta e_{2,} c_2^2, \alpha_2)$

   a. Function: Compute $\Delta p_2, \Delta e_2, c_2^2, \alpha_2$ given $\Delta\rho_1, \Delta e_1, \rho_2, \alpha_{min}$ and assuming an isentropic change of state.
   b. Description: Evaluate Equation (42) numerically using a 2 point Runge method. Use Equation (25) for parts of the change of state path where α=1.
   c. Algorithm:

      $F_1(\Delta\rho_1, \Delta e_1, \alpha_{min}) \rightarrow (\Delta p_1, c_1^2, \Delta p_{r_1}, \Delta e_{r_1})$
      If $\alpha_{\min} \leq 1$ CALL ISEMIE
      Else to numerically ntegrate Equation (42).

         apply a 2 point Runge-Kutta method,
         If α=1 after any step CALL ISEMIE to complete integration.

3. Subroutine HUGP_A:$F_3(\Delta\rho_1, \Delta e_1, \Delta\rho_2, \alpha_{min}) \rightarrow (\Delta p_2, \Delta e_{2,} c_2^2, \alpha_2)$

   a. Function: Compute $\Delta p_2, \Delta e_2, c_2^2, \alpha_2$ given $\Delta\rho_1, \Delta e_1, \Delta\rho_2, \alpha_{min}$ and assuming a change of state along the Hugoniot.
   b. Description: Use iteration to determine an α_2 which satisfies Equation (44).
   c. Algorithm:

      If $\alpha_{min} = 1$ Solve for final state with Equations (44)-(46) using $\alpha_1 = \alpha_2 = 1$.
      Perform Newton iteration onα_2 for final state using Equations (44)-(46).

4. Subroutine ISTP_A: $F_4(\Delta p_1, \Delta e_1, \alpha_{min}) \rightarrow (\Delta\rho_1, c_1^2, \alpha_1)$

   a. Function: Compute $\Delta\rho_1, c_1^2, \alpha_1$ given $\Delta p_1, \Delta e_1, \alpha_{min}$
   b. Description: Compute α using Equation (33) and the find the density by calling subroutine ISTMIE
   c. Algorithm:

      If $p \geq p_s$ *or* $\alpha_{min} = 1$ call ISTMIE to determine ρ_1 *and* c_1^2.
      Otherwise:

      Compute α from Equation (33) and $\Delta p_s = \alpha\Delta p + (\alpha - 1)p_\infty$
      $f_4(\Delta p_s, \Delta e_1) \rightarrow (\Delta\rho_s, c_t^2)$
      Compute $\Delta\rho = \frac{\Delta\rho_s}{\alpha} + \rho_\infty\left(\frac{1}{\alpha} - 1\right)$

5. Subroutine IISP_A: $F_5(\Delta p_1, \Delta e_1, \Delta p_2, \alpha_{min}) \rightarrow (\Delta\rho_2, \Delta e_2, c_2^2, \alpha_2)$

   a. Function: Compute $\rho_2, e_2, c_2^2, \alpha_2$ given $p_1, e_1, p_2, \alpha_{min}$ and assuming an isentropic change of state.
   b. Description: Numerically integrate Equation (42) from the initial state until target pressure is reached.
   c. Algorithm:

      - $F_4(\Delta p_1, \Delta e_1, \alpha_{min}) \rightarrow (\Delta\rho_1, c_1^{2^n})$
      - Integrate Equation (42) until p≥p$_2$

        Apply a 2 step Runge Kutta method.
        $F_1(\Delta\rho^n, \Delta e^{n-1}, \alpha_{min}) \rightarrow (\Delta p^n, c_t^2)$

      - Interpolate for:

$$\begin{aligned} \Delta\rho_2 &= \Delta\rho^n - \vartheta(\Delta\rho^n - \Delta\rho^{n-1}) \\ \Delta e_2 &= \Delta e^n - \vartheta\left(\frac{de}{d\rho}\right)^n \\ &where: \\ \vartheta &= \left(1 - \frac{\Delta p_2 - \Delta p^{n-1}}{\Delta p^n - \Delta p^{n-1}}\right) \end{aligned} \tag{3}$$

      - Compute final properties:$F_1(\Delta\rho_2, \Delta e_2, \alpha_{min}) \rightarrow (\Delta p_2, c_2^2)$

6. Subroutine IHUP_A: $F_6(\Delta p_1, \Delta e_1, \Delta p_2, \alpha_{min}) \rightarrow (\Delta\rho_2, \Delta e_2, c_2^2, \alpha_2)$

   a. Function: Compute $\rho_2, e_2, c_2^2, \alpha_2$ given $p_1, e_1, p_2, \alpha_{min}$ and assuming a change of state along the Hugoniot.

   b. Description: Compute α_1, α_2 using p_1, p_2 and Equation (33). Use a Newton iteration to solve Equation (44).

   c. Algorithm:

   - If α_{min}=1, material is fully compacted. Compute ρ_2, e_2, c_2^2 from $f_6(\Delta p_1, \Delta e_1, \Delta p_2) \rightarrow (\Delta p_2, \Delta e_2)$
   - Otherwise

     Compute α_1, α_2 using p_1, p_2 and Equation (33).
     Iterate for value of ρ_2 which satisfies Equation (33)

. . .

APPENDIX C
USER MANUAL PAGES

Name: MP_ALP
Indicates the number of P-α materials included in the calcualtion.

Default: MP_ALP= 0
Restrictions: MP_ALP≥0
Recommendation: none

Remarks:

Up to 9 P-α materials can be included in the calculation. The increased storage per cell is 2*MP_ALP. The reference and initial property for a P-α material is described in the same manner as other materials. Materials 91–95 are reserved for P-α equations of state while 96–99 are for Mie-Grueneisen Equation of state materials

Codeword: **EQSTPAR** (7/9)

Mie-Grueneisen Equation of State (96≤NM≤99)

$$p = p_r(\rho) + \Gamma_o \rho_o (e - e_r(\rho)) \tag{4}$$

See NSWC/TR–95/107 for definition of constants in equation.

Input parameters

pos	variable	internal name	accepted if
3	S	ESCAPA	always
4	c_s^2	ESCAPB	always
5	p_o	ESD	always
6	ρ_o	ESALPH	always
7	e_o	ESBETA	always
8	Γ_o	ESGAMM	always
9	p_{cav}	ESPCAV	!=0
10	$\Delta\rho_{max}$	DRHOMX	!=0
11	$\Delta\rho_{min}$	DRHOMN	!=0

Remarks:

The **EQSTPAR** section should preceed the **MATERIAL** section. To avoid confusion with existing material definitions, use NM=99 for Mie-Grueneisen materials defined using **EQSTPAR** section

Codeword: **EQSTPAR** (8/9)

P-α Equation of State (90≤NM≤95)

See NSWC/TR–95/107 for a definition of the P-α Equation of State.

Input parameters

pos	variable	internal name	accepted if
3	S	ESCAPA	always
4	c_s^2	ESCAPB	always
5	p_o	ESD	always
6	ρ_o	ESALPH	always
7	e_o	ESBETA	always
8	Γ_o	ESGAMM	always
9	α_o	ESDELT	always
10	Δp_S	ESES	always
11	c_e	ESESP	always
12	Δp_e	ESIOTA	always
13	p_{cav}	ESPCAV	!=0
14	$\Delta\rho_{max}$	DRHOMX	!=0
15	$\Delta\rho_{min}$	DRHOMN	!=0

Remarks:

The **EQSTPAR** section should preceed the **MATERIAL** section. To avoid confusion with existing material definitions, use NM=95 for Mie-Grueneisen materials defined using **EQSTPAR** section

APPENDIX D
STORAGE ARRYAS FOR EQUATIONS OF STATE PARAMETERS

The Mie-Grueneisen and P-α equations of state make use of a number of amterial constants. The following table provides a list of these variables using the symbols defined in the Glossary.

Internal Name	P-α constants	Mie-Gruneisen constant
ESCAPA	S	S
ESCAPB	c_s^2	c_s^2
ESCAPC	a_1	a_1
ESCAPD	a_2	a_2
ESA	a_3	a_3
ESB	a_4	a_4
ESC	a_5	a_5
ESD	p_o	p_o
ESALPH	ρ_o	ρ_o
ESBETA	e_o	e_o
ESGAMM	Γ_o	Γ_o
ESDELT	α_o	
ESES	Δp_s	
ESESP	c_e	
ESETA	Δp_e	
ESIOTA	α_e	
ESPCAV	p_{cav}	
DRHOMX	$\Delta\rho_{max}$	
DRHOMN	$\Delta\rho_{min}$	

APPENDIX E
COMPUTING THE P-α PARAMETERS FOR SAND

Sand consists of sand grain, water, and air. The air and water form a mixture which fills the pore spaces between the sand grains. The solid component of the P-α model represents the sand grain and water mixture, while the void simulates the air. To apply the P-α model to sand, the Mie-Grueneisen equation of state parameters for this solid component must be constructed from the known water and sand grain properties.

The information required to construct the Mie-Grueneisen constants for the grain-water mixture are:

1. The dry sand density, ρ_d
2. The saturation, s.
3. The following material properties for water and sand grain:
   a. Density, ρ.
   b. Sound speed, c.
   c. The MieGrueneisen Constants, Γ_o.
   d. The shock velocity verses particle velocity slope, S.
   e. Specific heat, C_v (optional for many applications).

The porosity, n, which is the volume fraction of the void, is given by:

$$n = \frac{(\rho_g - \rho_d)}{\rho_g} . \qquad \text{E- 1}$$

The density of the compacted sand with all of the air pore volume eliminated is:

$$\rho_{w+g} = \frac{(1-n)\rho_g + sn\rho_w}{1-(1-s)n} , \qquad \text{E- 2}$$

while the mass fractions of the grain and water components of this mixtures are

$$\lambda_w = \frac{sn\rho_w}{(1-n)\rho_g + sn\rho_w} \qquad \text{E- 3}$$

and

$$\lambda_g = \frac{(1-n)\rho_g}{(1-n)\rho_g + sn\rho_w} . \qquad \text{E- 4}$$

Furthermore, from Equations (E-2) to (E-4) it follows that

$$v_{g+w} = \lambda_g v_g + \lambda_w v_w , \qquad \text{E- 5}$$

where v is the specific volume.

The specific heat for the grain-water mixture follows directly from a mass average:

$$C_{v_{g+w}} = \lambda_g C_{v_g} + \lambda_w C_{v_w} \qquad \text{E- 6}$$

The speed of sound for the grain-water mixture arises from the definition:

$$c^2 = -v^2 \left(\frac{\partial p}{\partial v}\right)_s = -\frac{v^2}{\left(\frac{\partial v}{\partial p}\right)_s} . \qquad \text{E- 7}$$

Assuming that the water and grain components are always in pressure equilibrium, the denominator of Equations (E-5) can be evaluated by differentiating Equation (E-7), which yields:

$$-\left(\frac{\partial v}{\partial p}\right)_s = \frac{v_{g+w}}{c^2_{g+w}} = -\lambda_g\left(\frac{\partial v_g}{\partial p}\right)_s - \lambda_w\left(\frac{\partial v_w}{\partial p}\right)_s = \lambda_g\frac{v_g^2}{c_g^2} + \lambda_w\frac{v_w^2}{c_w^2} \qquad \text{E- 8}$$

Solving for the grain-water sound speed yields:

$$c^2_{g+w} = \frac{v^2_{g+w}}{\lambda_g\frac{v_g^2}{c_g^2} + \lambda_w\frac{v_w^2}{c_w^2}} = \frac{1}{\rho^2_{g+w}\left(\frac{\lambda_g}{c_g^2\rho_g^2} + \frac{\lambda_w}{c_w^2\rho_w^2}\right)} \qquad \text{E- 9}$$

The grain-water Γ also follows directly from the definition:

$$\Gamma = v\left(\frac{\partial e}{\partial p}\right)^{-1}_v \qquad \text{E- 10}$$

Noting that $e_{g+w} = \lambda_g e_g + \lambda_w e_w$ and differetiating with respect to p yields:

$$\Gamma_{g+w} = \frac{v_{g+w}}{\frac{\lambda_g v_g}{\Gamma_g} + \frac{\lambda_w v_w}{\Gamma_w}} = \frac{1}{\rho_{g+w}\left(\frac{\lambda_g}{\Gamma_g\rho_g} + \frac{\lambda_w}{\Gamma_w\rho_w}\right)}. \qquad \text{E- 11}$$

The final property of interest is S, the slope of the u_p verses u_s relation. This quantity is treated in a manner analogous to sound speed. Thus,

$$S^2_{g+w} = \frac{1}{\rho^2_{g+w}\left(\frac{\lambda_g}{S_g^2\rho_g^2} + \frac{\lambda_w}{S_w^2\rho_w^2}\right)} \qquad \text{E- 12}$$

DISTRIBUTION

	Copies
DOD ACTIVITIES (CONUS)	
DEFENCE TECHNICAL INFORMATION CENTER 8725 JOHN J KNIGMAN RD SUITE 0944 FT BELVIOR VA 22020-6218	12
ATTN 33 (S LEKOUDIS)	1
33 (G MAIN)	1
33 (D HOUSER)	1
OFFICE OF NAVAL RESEARCH BALLSTON TOWER 1 800 NORTH QUINCY STREET ARLINGTON VA 22217-5660	
ATTN SEA-03P3 (R BOWSER)	1
SEA-03P33 (P WU)	1
PMO-407 (W HINCKLEY)	1
COMMANDER NAVAL SEA SYSTEMS COMMAND 2531 JEFFERSON DAVIS HIGHWAY ARLINGTON VA 22242-5160	
ATTN P7 (R KAVETSKY)	1
40E (E JOHNSON)	1
4140 (R GARRETT)	1
4140 (R JONES)	1
420 (L TAYLOR)	1
4201 (R MCKEOWN)	3
4210 (D TAM)	1
4220 (J BURNS)	1
4220 (D NELL)	1
4220 (D BETANCOURT)	1
4220 (H CHEN)	1
4220 (J MCKIRGAN)	1
4220 (W WALKER)	1
4610 (H MAIR)	1
4620 (D HAN)	1
4620 (K KIDDY)	1
4630 (G HARRIS)	1
ATTN 911 (J GOLDWASSER)	1
9210 (R GUIRGUIS)	1
COMMANDER INDIAN HEAD DIVISION NAVAL SURFACE WARFARE CENTER SILVER SPRING MD 20903-5640	
ATTN TECHNICAL LIBRARY	1
67.1 (C MILLIGAN)	1
67.1 (S ZILLIACUS)	1
COMMANDER CARDEROCK DIVISION NAVAL SURFACE WARFARE CENTER 9500 MACARTHUR BLVD BETHESDA MD 20084-5000	
ATTN TECHNICAL LIBRARY	1
6400 (J P BORIS)	1
6440 (M EMERY)	1
NAVAL RESEARCH LABORATORY 4555 OVERLOOK DR SW WASHINGTON DC 20375-5320	
ATTN TECHNICAL LIBRARY	1
69SG (Y KWON)	1
69SG (Y SHIN)	1
SUPERINTENDENT NAVAL POSTGRADUATE SCHOOL MONTEREY CA 93940	
ATTN TECHNICAL LIBRARY	1
SPSD (K GOERING)	1
SPSD (D BRUDER)	1
SPSD (M GILTRUD)	1
DIRECTOR DEFENSE NUCLEAR AGENCY 6801 TELEGRAPH RD. ALEXANDRIA VA 22310-3398	
ATTN CODE 10 (G KEKELIS)	1
COMMANDER COSTAL SYSTEMS STATION DAHLGREN DIVISION NAVAL SURFACE WARFARE CENTER 6703 WEST HIGHWAY 98 PANAMA CITY FL 32407-7001	

DISTRIBUTION (Continued)

	Copies
ATTN MNMW (J COLLINS)	1
MNMW (J FOSTER)	1
WRIGHT LABORATORY	
EGLIN AFB FL 32542-5434	
ATTN TECHNICAL LIBRARY	1
WT-PD (S WILKERSON)	1
WT-TC (K KIMSEY)	1
WT-TD (G RANDERS-PEHRSON)	1
DIRECTOR	
U.S. ARMY RESEARCH LAB	
APG MD 21005-5066	
NON-DOD ACTIVITIES	
CENTER FOR NAVAL ANALYSES	
4401 FORD AVENUE	
ALEXANDRIA VA 22302-0268	1
ATTN GIFT AND EXCHANGE	4
LIBRARY OF CONGRESS	
WASHINGTON DC 20540	
ATTN TECHNICAL LIBRARY	1
B216 (B A KASHIWA)	1
F663 (T ADAMS)	1
J576 (M LEWIS)	1
J576 (D RABERN)	1
LOS ALAMOS NATIONAL LABORATORY	
PO BOX 1663	
LOS ALAMOS NM 87545	
ATTN 1425 (S. ATTAWAY)	1
1431 (J.M. MCGLAUN)	1
1431 (E.S. HERTEL)	1
1432 (S. SILLING)	1
1542 (P. YARRINGTON)	1
7141 (TECHNICAL LIBRARY)	1
SANDIA NATIONAL LABORATORIES	
PO BOX 5800	
ALBUQUERQUE NM 87185-5800	

	Copies
ATTN TECHNICAL LIBRARY	1
8742 (J J DIKE)	1
8742 (V REVELLI)	1
8742 (L WEINGARTEN)	1
SANDIA NATIONAL LABORATORIES	
PO BOX 969	
LIVERMORE CA 94551-0969	
ATTN L-313 (LIBRARY)	1
L-35 (R COUCH)	1
L-84 (K ROSENKILDE)	1
LAWRENCE LIVERMORE	
NATIONAL LABORATORY	
PO BOX 808	
LIVERMORE CA 94550-0622	
ATTN T GEERS	1
MECHANICAL ENGINEERING	
UNIVERSITY OF COLORADO	
BOULDER CO 80309-0427	
ATTN 0411 (D BENSON)	1
DEPT OF AMES	
UNIVERSITY OF CALIFORNIA	
LA JOLLA CA 92093-0411	
ATTN R LOHNER	1
GEORGE MASON UNIVERSITY	
FAIRFAX VA 22030-4444	
ATTN T BELYTSCHKO	1
MECHANICAL ENGINEERING	
NORTHWESTERN UNIVERSITY	
2145 SHERIDAN RD	
EVANSTON IL 60208-3111	
ATTN T J R HUGHES	1
MECHANICAL ENGINEERING	
STANFORD UNIVERSITY	
PALO ALTO CA 94306	
ATTN A PROSPERETTI	1
MECHANICAL ENGINEERING	
JOHNS HOPKINS UNIVERSITY	
BALTIMORE MD 21218	

DISTRIBUTION (Continued)

	Copies
ATTN J STUHMILLER	1
JAYCOR	
11011 TORREYANA RD	
PO BOX 85154	
SAN DIEGO CA 92138-9259	
ATTN K KAN	1
JAYCOR	
1608 SPRING HILL RD	
VIENNA VA 22182-2270	
ATTN: G L CHAHINE	1
R DURAISWAMI	1
K M KALUMUCK	1
DYNAFLOW INC	
7210 PINDELL SCHOOL RD	
FULTON MD 20759	
ATTN J DERUNTZ	1
USA	
19875 INDIAN SUMMER LANE	
MONUMENT CO 80132	
ATTN J ENIG	1
ENIG ASSOCIATES	
11120 NEW HAMPSHIRE AVE	
SUITE 500	
SILVER SPRING MD 20904-2633	
ATTN V GODINO	1
. LITTLEWOOD	1
A&T ENGINEERING TECH CENTER	
240 ORAL SCHOOL RD SUITE 105	
MYSTIC CT 06355-1208	
ATTN M BARON	1
R ATKATSH	1
R DADDAZIO	1
I SANDLER	1
R SMILOWITZ	1
WEIDLINGER ASSOCIATES	
333 SEVENTH AV	
NEW YORK NY 10001	
ATTN K STULTZ	1
WEIDLINGER ASSOCIATES	
1735 JEFFERSON DAVIS HWY	
SUITE 1002	
ARLINGTON VA 22202	

	Copies
ATTN G JOHNSON	1
ALLIANT TECHSYSTEMS INC	
MN11-2925	
600 SECOND ST NE	
HOPKINS MN 554343	
ATTN J HALLQUIST	1
D STILLMAN	1
LSTC	
2876 WAVERLEY WAY	
LIVERMORE CA 94550	
ATTN MS 2-3-1 (J. BAUM)	1
SAIC	
1710 GOODRIDGE DR	
MCLEAN VA 22102	
ATTN R BRITT	1
SAIC	
P O BOX 469	
ST JOSEPH LA 71366-0469	
ATTN O DENGEL	1
ROUTE 1 BOX 200	
FRONT ROYAL VA 22630	
ATTN D CURTIS	1
T MOYER	1
R MILLER	1
NKF ENGINEERING	
4200 WILSON BLVD SUITE 900	
ARLINGTON VA 22203-1800	
NON-DOD ACTIVITIES (EX-CONUS)	
ATTN K FLORIE	1
MACNEAL-SCHWENDLER CORP	
GRONINGENWEG	6
2803 PV GOUDA	
THE NETHERLANDS	

DISTRIBUTION (Continued)

	Copies
ATTN J GREENHORN	1
R HAXTON	1
DRA ST LEONARDS HILL	
DUNFERMLINE FIFE KY11 5PW	
SCOTLAND UNITED KINGDOM	
ATTN I CULLIS	1
DRA FT HALSTEAD	
SEVENOAKS KENT TN14 7BP	
ENGLAND UNITED KINGDOM	
ATTN J BLAKE	1
MATHEMATICS AND STATISTICS	
UNIVERSITY OF BIRMINGHAM	
EDGBASTON	
BIRMINGHAM BI5 2TT	
ENGLAND UNITED KINGDOM	
ATTN D RITZEL	1
DRE SUFFIELD	
BOX 4000	
MEDICINE HAT ALBERTA T1A 8K6	
CANADA	
ATTN J P BEST	1
UNDERWATER SYSTEMS DIVISION	
MATERIALS RESEARCH LAB	
PO BOX 50	
ASCOT VALE VIC 3032 AUSTRALIA	

	Copies
ATTN P CLASSEN	1
U. VOGEL	1
BMVG R T II 3	
POSTFACH 1328	
DW-53003 BONN 1 GERMANY	
ATTN J FREERCKS	1
BWB-SG14	
POSTFACH 7360	
D-56068 KOBLENZ 1 GERMANY	
ATTN W RYBAKOWSKI	1
WTD-71	
BERLINERSTRASSE 115	
D-24340 ECKERNFRDE GERMANY	
ATTN MOD/WSB	
TA (B FIESSLER)	1
TAF (H J DIEKHOFF)	1
TAF (E WACHSMANN)	1
IABG	
EINSTEINSTRASSE 20	
D-85521 OTTOBRUNN GERMANY	
INTERNAL	
E231	3
B (M LACEY)	1
B40 (C LARSON)	1
B44 (T ZIEN)	1
B44 (. WARDLAW)	10